REPORT DOCUMENTATION PAGE

Form Approved
OMB No. 0704-0188

1. REPORT DATE *(DD-MM-YYYY)*	2. REPORT TYPE	3. DATES COVERED *(From - To)*
12-05-2010		

4. TITLE AND SUBTITLE

The Effects of Thermal Barrier Coating, Common-Rail Injection, and Reduced Compression Ratio on the Efficiency of Single-Cylinder Diesel Engines

5a. CONTRACT NUMBER

5b. GRANT NUMBER

5c. PROGRAM ELEMENT NUMBER

6. AUTHOR(S)
Arment, Tyrell Wayne

5d. PROJECT NUMBER

5e. TASK NUMBER

5f. WORK UNIT NUMBER

7. PERFORMING ORGANIZATION NAME(S) AND ADDRESS(ES)

8. PERFORMING ORGANIZATION REPORT NUMBER

9. SPONSORING/MONITORING AGENCY NAME(S) AND ADDRESS(ES)

U.S. Naval Academy
Annapolis, MD 21402

10. SPONSOR/MONITOR'S ACRONYM(S)

11. SPONSOR/MONITOR'S REPORT NUMBER(S)

Trident Scholar Report no. 385 (2010)

12. DISTRIBUTION/AVAILABILITY STATEMENT

This document has been approved for public release; its distribution is UNLIMITED

13. SUPPLEMENTARY NOTES

14. ABSTRACT

This study considers the relatively high fuel consumption of small-displacement Diesel engines and seeks to determine if fuel consumption can be improved through the combined use of thin ceramic thermal barrier coatings, reduced compression ratio, and the use of a high pressure common-rail fuel injection system. A small displacement (219 cc) single-cylinder direct-injection production Diesel engine is utilized. A Ricardo WAVE simulation is developed and suggests that through simultaneous application of the coatings and reduction of compression ratio, the fuel consumption can be improved through a reduction in thermal losses.

15. SUBJECT TERMS

Small displacement Diesel engine, fuel consumption, fuel efficiency, Ricardo WAVE simulation, common rail injection, ceramic thermal barrier

16. SECURITY CLASSIFICATION OF:			17. LIMITATION OF ABSTRACT	18. NUMBER OF PAGES	19a. NAME OF RESPONSIBLE PERSON
a. REPORT	b. ABSTRACT	c. THIS PAGE		96	19b. TELEPHONE NUMBER *(Include area code)*

ABSTRACT

This study considers the relatively high fuel consumption of small-displacement Diesel engines and seeks to improve it through thin ceramic **thermal barrier coatings**. A small displacement (219 cc) single-cylinder direct-injection production Diesel engine is utilized. A Ricardo WAVE simulation is developed and suggests that through simultaneous application of the coatings and reduction of **compression ratio**, the fuel consumption can be improved through a reduction in thermal losses. At the stock compression ratio, the application of thermal barrier coatings does not improve fuel consumption unless injection timing is carefully controlled. When injection timing is also adjusted, fuel consumption can be improved by up to 10%, particularly at low loads, with application of the thermal barrier coatings. The data show higher rates of energy release, higher peak pressures, leading to the lower fuel consumption. When coatings are combined with simultaneous reduction in compression ratio and injection timing adjustment, fuel consumption remained similar at low loads but increased at high loads due to delayed combustion phasing and increased exhaust sensible **enthalpy** loss. However, these data suggest that an engine with lower compression ratio could achieve similar fuel consumption with thermal barrier coatings, thus allowing a smaller and lighter engine to be utilized. A common-rail fuel injection system was also utilized to test the effects of high pressure fuel injection. While gross fuel consumption suffered due to an oversized fuel injector, the data did show a direct correlation of efficiency to fuel droplet size.

Acknowledgments

This project has been one of the most challenging and rewarding experiences of my academic career so far. It would never have been possible to complete without the knowledge, skill, and patient support of all those who aided me along the way. The amount of credit these people deserve greatly outweighs the significance of simply listing their names the acknowledgements.

Machine Shop
- Brandon Stanley
- Matt Stanley
- Mike Superczynski

Systems Lab
- Joe Bradshaw

Engines Lab
- Charlie Baesch
- John Hein

NAVAIR-China Lake
- Mr. John Caufield
- Mr. Ferguson Ayers

Office of Naval Research
- Dr. Dave Shifler

Associate Professor Jim S. Cowart
Assistant Professor Patrick Caton
CAPT Leonard J. Hamilton, USN

Table of Contents

List of Figures

List of Tables

List of Symbols

ATC: .....After Top Center

A(θ): .....Area at CAD (θ) (m^2)

A_n: .....Nozzle Shape Coefficient

$A_{top/bottom}$: .....Area of Either the Top or Bottom of the Cylinder (m^2)

B: .....Cylinder Bore Diameter (m)

B_f: .....Volume of Fuel Injected (m^3)

BMEP: .....Brake Mean Effective Pressure

BSFC: .....Brake Specific Fuel Consumption

C_1: .....Correction factor for Mean Piston Speed

CAD: .....Crank Angle Degree

c_p: .....Constant Pressure Specific Heat (kJ/kg-K)

CR: .....Compression Ratio

c_v: .....Constant Volume Specific Heat (kJ/kg-K)

d_{cyl}: .....Diameter of the Cylinder, the Bore Diameter (m)

FMEP: .....Friction Mean Effective Pressure

h_{exh}: .....Enthalpy of the Exhaust Gases (kJ/kg-K)

h(θ): .....Heat Transfer Coefficient at CAD (θ)

HR: .....Heat Release

HTM: .....Heat Transfer Multiplier

IMEP: .....Indicated Mean Effective Pressure

K: .....Gain for Pressure Transducer Voltage

k: .....Ratio of c_p/c_v

L_{conrod}:.....Length of the connecting rod (cm)

L_{strk_rad}: .....Radius of the Stroke (cm)

LHR: .....Low Heat Rejection

m_{air}: .....Mass of Air in the Cylinder (kg)

m_{fuel}: .....Mass of Fuel (kg)

m_{total}:.....Total Mass of Air and Fuel Present in the Cylinder (kg)

MBT:.....Maximum Brake Torque

M_{XX}: .....Molar Mass of Compound XX (kg/kmol)

$P(\theta)$:.....Pressure at CAD (θ)

ΔP_{inj}:.....Difference in Pressure from the Fuel System to the Cylinder (Pa)

p: .....Same as $P(\theta)$

PPLOC: .....Peak Pressure Location

δQ_{ER} : .....Differential Energy Release (J/CAD)

$Q_{exhaust}$: .....Heat Loss Through the Exhaust Manifold (J)

Q_{fuel}: .....Heat Added from the Fuel (J)

δQ_{wall} : .....Differential Energy Loss to the Wall (J/CAD)

Q_{wall}: .....Heat Loss to the Wall (J)

R:.....Ratio of Connecting Rod Length to Stroke Radius

rad: .....Radians

R_{air}:.....Gas Constant for Air (J/kg-K)

ρ_a: .....Air Density (kg/m^3)

$\overline{S_p}$:.....Mean Piston Speed (m/s)

SOI:.....Start of Injection

$T(\theta)$: .....Average Temperature in the Cylinder at CAD (θ)

$\Delta T(\theta)$:.....Temperature Difference Between Combustion Gases and Atm. (K)

TBC:.....Thermal Barrier Coatings

TDC: .....Top Dead Center

V_c: .....Clearance Volume (m^3)

Volt(θ):.....Voltage at CAD (θ)

V(θ): .....Volume of the Cylinder at CAD (θ)

W:.....Mechanical Work, PΔV

w:.....Corrected Average Piston Speed for **Woschni Correlation** (m/s)

$\bar{x}_{32}$:.....Sauter Mean Diamter (m)

Y_{XX}:.....Molar Fraction of Compound XX

1 Introduction and Background

Small internal combustion engines typically have poor efficiency and poor performance (maximum **Brake Mean Effective Pressure**, BMEP) relative to larger automotive and truck engines. Other classes of engines, notably in motorsports, have outstanding performance, often with poor efficiency. Engines associated with hybrid vehicles have excellent efficiency, often with lower performance. The dual deficiency of very small-displacement engines is unique. Even diesel engines, generally noted for their high fuel conversion efficiency, often suffer from poor **Brake Specific Fuel Consumption** (BSFC) on the smallest scales.

This study seeks to improve the fuel efficiency (BSFC) of a small production diesel engine. The engine chosen for this study is the Yanmar L48V with a peak output power of only 3 kW. This engine is one of the smallest widely available production Diesel engines. Figure 1 shows the peak BMEP of this engine as compared to some other naturally-aspirated, mechanically-injected automotive Diesel engines [3]. The small Yanmar has a high Compression Ratio (CR), nominally 21:1. This comparison shows that the BMEP of the Yanmar engine is well below that of the larger automotives Diesels produced throughout the United States, Europe, and Asia. There are two main hypotheses that attempt to explain why this high-CR, small-displacement Diesel engine is so inefficient at producing the same amount of torque per unit volume as automotive engines.

The two hypotheses for this deficiency were proposed by Heywood. One issue that drops the power output of this engine is the significance of crevice volume at high compression ratio [8], [1]. In general, the area inside the crevice volume is cooler than the rest of the combustion chamber and is not exposed to the flame. Because of this colder temperature, a significant amount of unburned hydrocarbons can escape combustion, reducing the amount of fuel energy that can be consumed by the flame during the combustion event and reducing the performance of the engine. As the compression ratio of an engine is increased, the relative significance of the crevice volume is also increased due to the very small **clearance volume**. While this effect would be strongest for homogenous gasoline engines, it may also be an issue with small high CR diesel engines.

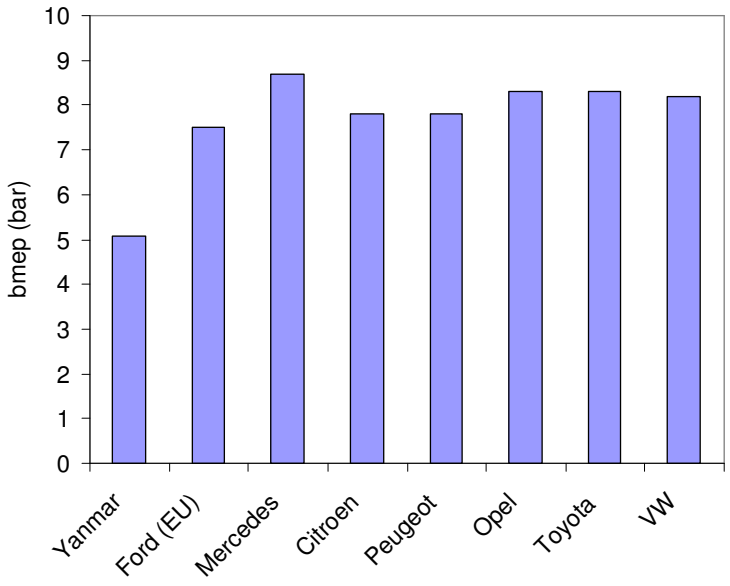

Figure 1: Best Torque (BMEP) Comparison of Various Mechanically Injected Naturally Aspirate Diesel Engines

Heywood also suggests that large surface-area-to-volume ratio of high CR engines impacts efficiency through increased thermal losses [8]. Data from Heywood from mechanically injected diesel engines like the Yanmar engine used in this study were used to create Figure 2, which shows the variation of BSFC versus engine displacement for many engines. Also shown in this graph are the calculated surface-area-to-volume ratios of these engines, using either a cylindrical or spherical approximation to the combustion chamber. The surface-area-to-volume ratio was calculated using the volume at top center for each engine because this location is where the maximum heat transfer occurs during combustion. The cylindrical approximation used the bore as the cylinder's diameter, while the spherical approximation derived a radius of a perfect sphere using the volume at top center. It can be seen that the relative importance of combustion chamber surface area becomes increasingly significant as engine displacement becomes small. This Figure suggests that combustion heat losses may be responsible for both the deficiency in engine performance and efficiency.

In order to counteract the negative effects of the relative crevice volume importance and the high surface-area-to-volume ratio that is present due to the high CR of small diesel engines, a two-fold approach involving the use of thermal barrier coatings and CR lowering was used in this study. The use of Thermal Barrier Coatings (TBC) to convert engines into **Low Heat Rejection** (LHR) engines has been studied in depth over the past decades (notably in the early 1980's) and many of these studies have reported a decrease in BSFC [10], [7], [12] on the order of 2-7%. Very few, if any, of these studies focused on creating a LHR engine with a displacement as small as the one in this study.

Published work involving the reduction in compression ratio is also somewhat limited. Heywood [8] shows that the theoretical efficiency of a spark-ignition engine would peak at a compression ratio of approximately 16:1 and then gradually begin to fall off due to the increased importance

of in-cylinder heat transfer with further increases in CR. It is reasonable to assume that a similar maximum in diesel engine efficiency with CR should exist. Parlak et al. [11] conducted a study involving both the reduction in compression ratio and the application of thermal barrier coatings and showed improvements in the low load-low speed and high load-low speed range. This study was conducted on a Diesel engine with displacement more than twice that of the Yanmar with engine speeds much lower than that in this study.

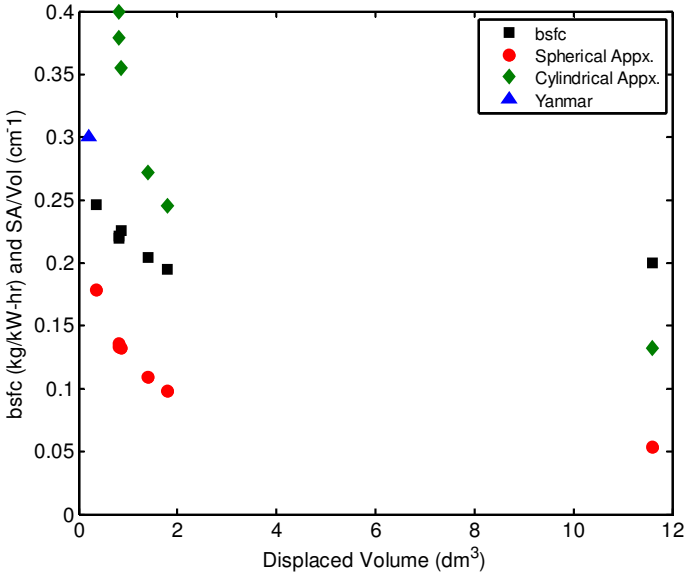

Figure 2: Best-Minimum BSFC Data for a Range of Engine Sizes, Including the Current Yanmar L48V. Also Shown are Analytic Results of Surface Area to Volume of These Engines Assuming Both a Sperical and Cylindrical Combustion Chamber

Other works [3], [10], [6] also indicate that fuel consumption can be decreased by increasing the fuel injection pressure. By increasing the injection pressure, the fuel becomes more finely atomized according to Equation (1) [3]:

$$\bar{x}_{32} = A_n \left(\Delta P_{inj}\right)^{-0.135} \left(\rho_a\right)^{0.121} \left(B_f\right)^{0.131} \tag{1}$$

According to this equation, the **Sauter mean diameter**, average fuel droplet size, should decrease as injection pressure increases. A decrease in droplet diameter would effectively increase the droplet's surface area to volume ratio, resulting in a faster, more complete burn. Higher pressure also imparts more momentum to the fuel causing it to penetrate the combustion chamber further, resulting in a more homogenous fuel mixture and uniform burn throughout the combustion chamber.

An important engine variable in this study involves tuning and optimizing the **Start Of Injection** (SOI) timing. Previous work with TBC engine parts has shown the need to modify SOI timing with the addition of TBC engine parts [10], [12], [9]. Thus, as engine changes were made in this study, the SOI was adjusted mechanically during testing of the CR and TBC by shimming the

fuel pump until a minimum BSFC was achieved. Once the common-rail system was fitted to the engine, the SOI was adjusted electronically.

A Ricardo WAVE simulation, further described in Appendix B.4, was developed to evaluate the simultaneous reduction in compression ratio and application of thermal barrier coatings. The results are shown in Figure 3. The Figure shows the variation of fuel consumption (BSFC, vertical axis) with compression ratio (horizontal axis) parameterized by the magnitude of heat transfer. The latter was quantified by a **heat transfer multiplier** (HTM), such that a value of 1.0 represents the heat transfer characteristics of a nominal automotive Diesel engine. As the HTM increases above unity, the in-cylinder heat transfer increases: for values less than unity, the engine becomes more adiabatic. The stock Yanmar engine operated in the upper-right hand section of this plot (CR21 with light load bsfc = 500 gm/kW-hr), which was determined experimentally by finding the Yanmar's low-load BSFC and intersecting that value with the known compression ratio. Thus, the stock Yanmar engine was found to have a HTM great than unity.

The Ricardo WAVE simulation highlights two paths that can be taken to decrease the BSFC of this Yanmar engine. First, the CR can be reduced, causing the engine performance to follow along the contour lines of constant HTM. Because of the original operating point on this plot, a reduced compression ratio could actually decrease the fuel consumption. This finding is counterintuitive to the classic result from analysis of an adiabatic engine, which is not specifically shown, however its trend follows below bottom (nearly adiabatic, HTM = 0.25) contour on Figure 3. The opposite is expected from the Yanmar engine due to its relatively large surface-area-to-volume ratio and enhance thermal losses in its stock configuration.

A second path to decreasing the BSFC is to decrease the HTM. This can be accomplished by insulating the combustion chamber using ceramic materials. A combination of reducing the CR and adding thermal barrier coatings would act together to move the operating point down and to the left, in effect yielding a synergistic result with a lower BSFC than could be achieved by either a reduction in CR or the addition of thermal barrier coatings alone.

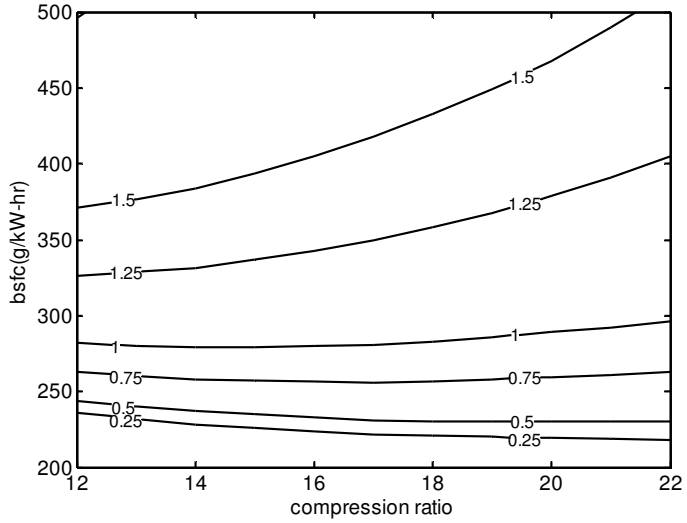

Figure 3: Ricardo WAVE Analysis of the Yanmar L48V at a Light-Mid Load Condition.

Thus the objective of this study is to analyze approaches that can be implemented to increase the efficiency of a small production diesel engine. The difference between this study and previous works is that, to the authors' knowledge, the techniques being implemented have rarely been combined, studied, and published on an engine of this size.

2 Experimental Setup

2.1 Engine Specifications

The engine being used in this study is the Yanmar L48V Diesel engine. The specifications on this engine are detailed in Table 1.

Engine type	**Yanmar L48V**
Cylinders	1
Stoke (mm)	57
Bore (mm)	70
Displacement (cc)	219
Compression Ratio	16-20.6
Engine Speed (rpm)	2750
Fuel	Diesel 2
Net Power ([kW]/rpm)	[3.1]/3600

Table 1: Engine Data

2.2 Instrumentation

This section outlines the instrumentation fitted to the Yanmar L48V Diesel engine, in order to facilitate a first law energy flow analysis. Some emissions data were also collected during testing to facilitate and analyze combustion efficiency. The engine used in this study was a four-stroke, naturally aspirated, single cylinder Diesel engine. The block diagram for the engine setup is shown in Figure 4. The Yanmar was coupled to a Model 66 Midwest and Dynamatic Eddy Current **dynamometer**. The dynamometer was controlled with a Dyne Systems Inter-Loc Controller.

The tests were conducted at variable loads, variable injection timing, a constant engine speed of 2750 rpm, and at three compression ratios: 21, 18, 16. The engine speed was chosen in order to simulate mid-Power performance. The compression ratio was altered by varying the head gasket thickness from 0.4 to 1.3 mm. Injection timing was adjusted at each compression ratio to optimize the efficiency of the engine by varying the thickness of the shims under the fuel pump.

After baseline engine data were collected on the performance of the stock engine, the same tests were performed on the engine at each of the lower compression ratios, with injection timing adjusted at each CR. The same tests were performed on the engine with a 0.381 mm thick yttrium stabilized zirconium ceramic coating on the face of the piston, head, and valves.

Finally a common-rail injection test platform was constructed to evaluate the effects various injection pressures had on fuel consumption. An automotive common-rail system, taken from a

Volkswagen Jetta, was adapted to the Yanmar engine and injection pressure was varied at near-constant load level at CR 21, TBC. A detailed description of its construction can be seen in Appendix E.4.

Piezo-electric pressure transducers were placed in the head (Kistler 6052C) and the fuel line (Kistler 4067) to gain data on in-cylinder pressure and start of injection data respectively. A thermocouple was placed in the exhaust manifold to measure exhaust gas temperature to an accuracy of ±0.1°C. Fuel consumption was measured by observing the volume of fuel consumed in a graduated cylinder during a measured period of time. Air flow was measured using a damper tank and differential pressure device (Meriam LFE). Exhaust gas composition data were collected using an infrared and chemical 5-gas analyzer (IM Type InfraRed Industries). All measurements were taken at various load levels after the engine was allowed to stabilize.

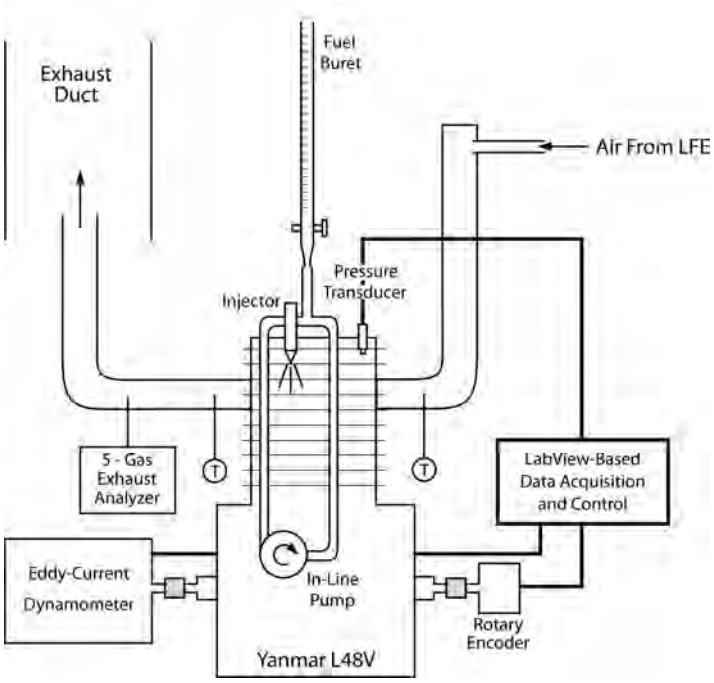

Figure 4: Experimental Engine-Dynamometer Schematic

3 Experimental Results

Initial experiments in this study investigated first the effect of reduced CR on the performance and efficiency of the Yanmar engine initially without TBC parts. It was anticipated that a reduction in CR would lead to later combustion phasing and thus the injection timing was advanced modestly (using thinner Yanmar replacement part injection pump shims) 3 degrees for CR 18 and 5 degrees for CR16. A load sweep was also performed at CR21 with 1.5 degrees of injection advance, showing no improvement in BSFC. These results show that the stock Yanmar engine injection timing was appropriately set for best torque. The results of the load sweep at 2750 rpm for all three CR tested are shown in Figure 5. It is evident that as the CR is reduced the BSFC curve shifts upwards, indicating greater fuel consumption (or lower thermal efficiency). Additionally, as CR is reduced the maximum torque developed at a given CR reduces as CR is reduced. The highest load at each CR corresponds to nominally 2% exhaust CO.

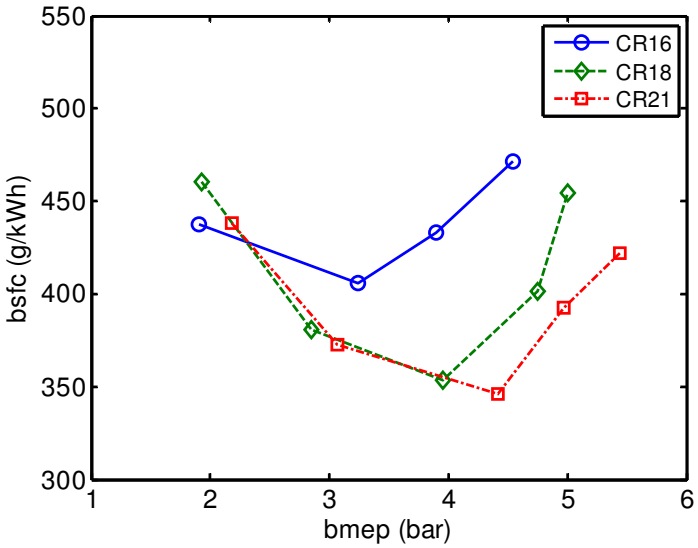

Figure 5: The Effect of Reduced Compression on the Stock Yanmar Engine. Injection Advanced 3 and 5 Degrees, Respectively for CR18 and CR16.

This trend of worsening fuel consumption with reduced compression ratio was not predicted by the Ricardo WAVE analysis. The WAVE analysis assumed constant combustion phasing, however, with this empirical data in Figure 5 the nominal **Peak Pressure LOCation** (PPLOC) shifted later and less optimally from 7 to 9 to 11 degrees **After Top Center** (ATC) when reducing CR from 21 to 18 to 16. Thus, even despite some modest injection advance with reduced CR, clearly greater injection advance is required in order to obtain optimum combustion phasing. Thus, in preparation for following experiments with the TBC engine parts, the injection pump base plate was ground down 0.6mm to allow for an additional 6 degrees of injection advance.

The second objective of this study was to evaluate the effect of TBC engine parts on engine efficiency. Initial experiments were performed at CR21 with both uncoated parts as well as TBC engine parts at the stock engine injection advance. The results are shown in Figure 6. Again the anticipated effect was not seen as fuel consumption worsened across the load range with the TBC engine parts. In-cylinder pressure traces revealed that combustion phasing was again not constant, but rather delayed with the TBC parts. PPLOC was retarded by nominally 3 degrees as compared to the stock engine. Exhaust temperatures also were higher by 10-25^{o}C for the TBC engine experiments. Thus again combustion phasing as controlled by injection timing was revealed as a critical control parameter to be optimized.

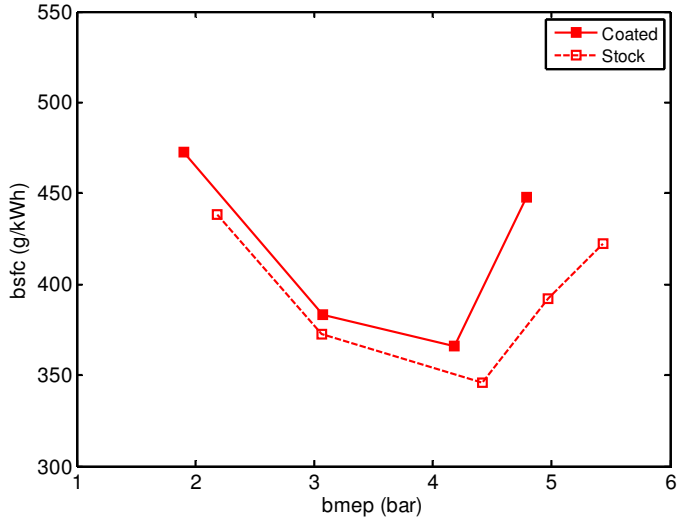

Figure 6: Load sweep at CR21 with Uncoated and Coated Engine Parts with Stock Injection Timing.

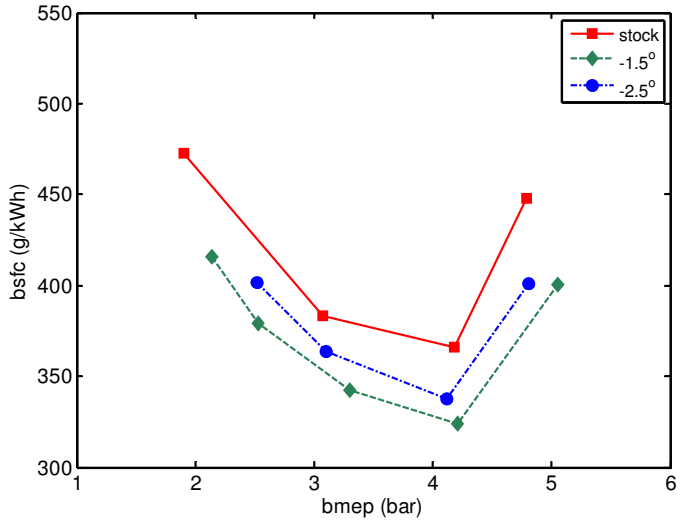

Figure 7: TBC Engine Tests at CR21 with Stock Injection as well as Advanced 1.5 deg and 2.5 deg.

Injection timing sweeps were next performed at CR21 in order to discover if improvements in combustion phasing could be made. Might there be a more ideal **Maximum Brake Torque** (MBT) injection timing with the TBC parts? These injection timing load sweeps at CR21 with the TBC engine parts are shown in Figure 7. PPLOC data shows that the Angle of Peak (AOP) advanced by nominally 1.5 deg with 1.5 degrees of injection advance, while another degree of advance provided slightly less than one degree of further combustion advance as evidenced by PPLOC.

It is clear from the data that advancing the injection timing by these very modest amounts at CR21 with TBC parts has a significant effect on engine performance and efficiency. By advancing injection timing by just 1.5 degrees the BSFC reduces (improves) by nearly ten percent. Thus injection timing is sensitive and must be optimized for engine operation with TBC parts.

Representative pressure traces for these three cases are shown in Figure 8. PPLOC for the MBT injection timing case is nominally 7-8 degATC. The most advanced pressure trace shows PPLOC approximately 5 deg ATC, however, also it can be seen that the pressure during the later stages of compression (<360degTC) is also higher due to early **heat release** adding to the compression work and thus worse fuel consumption and efficiency.

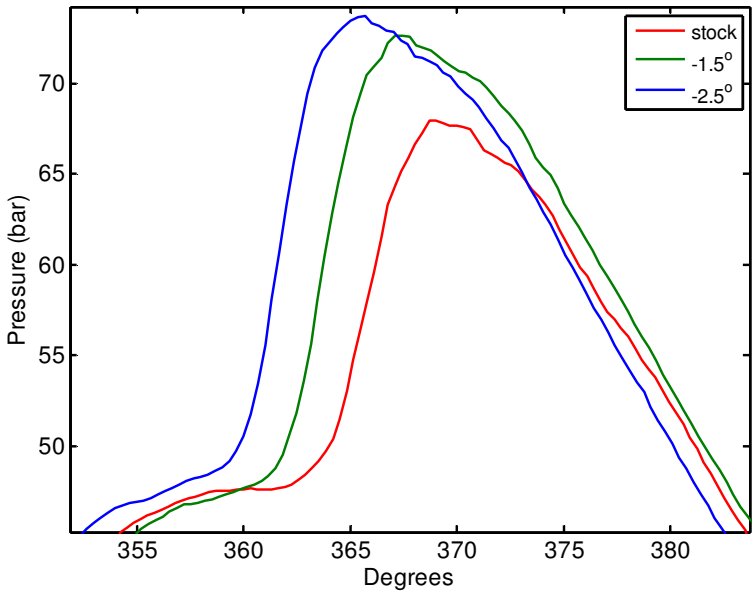

Figure 8: CR21 with TBC Engine Parts. Representative Pressure Traces for Stock Timing as well as Two Advanced Cases.

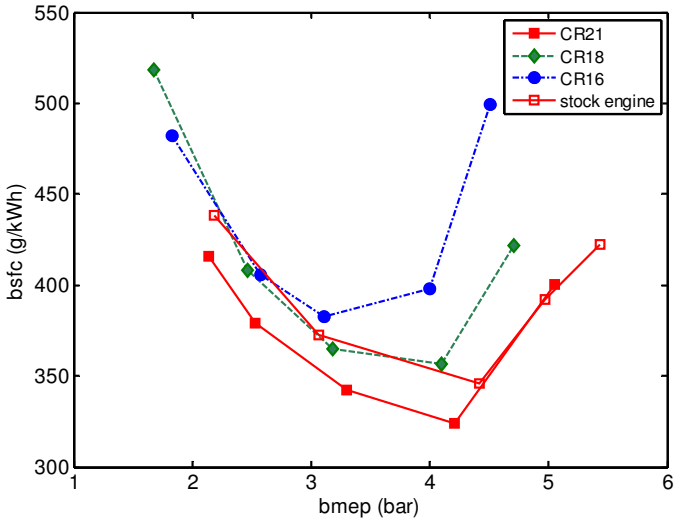

Figure 9: Stock Engine Data Compared to the Coated Engine with Optimized SOI at each CR

Similar injection timing adjustments (optimizations) and load sweeps were performed at the lower CRs. Four to five different injection timing settings were investigated at each CR in order to discover MBT timing. The final results of this study with optimized injection timing for CR16, 18 and 21 with TBC parts is shown in Figure 9. The stock engine (optimized timing) results are also shown in this Figure. It is clear that the TBC engine parts at CR21 provide a clear advantage over the low-mid load range approaching a ten percent improvement. At the high engine loads, both uncoated and coated parts show similar performance. There is a worsening, in general, of BSFC with reduced CR for the coated parts. However, again in the low-mid load regime both the CR16 and 18 TBC parts provide comparable performance to the stock CR21. Thus lower CR potential is possible with coated engine parts to provide similar performance to the stock engine in the low-mid load regime.

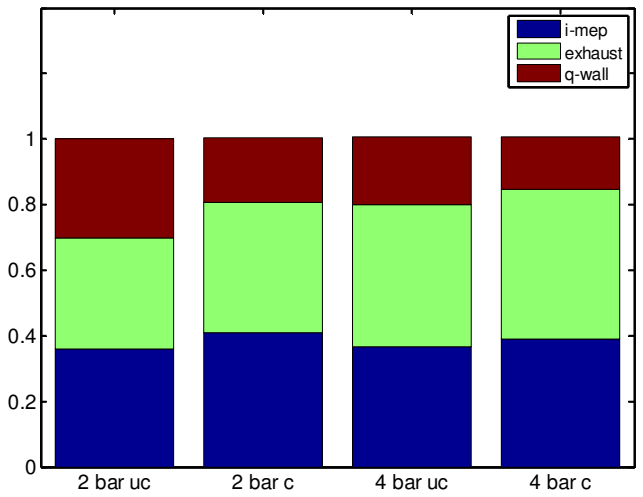

Figure 10: First Law Analysis of CR 21 TBC vs. Uncoated Configuration

A first law analysis [5][4] was carried out at two load settings for CR 21 coated and uncoated engine configuration and is shown in Figure 10. The total fuel energy is divided into three main divisions, Indicated Mean Effective Pressure (IMEP: gross in this study), exhaust enthalpy, and heat released through the engine walls (q-wall). In this analysis all the chemical energy in the exhaust (e.g. unburned hydrocarbons, soot and CO), is lumped in with the q-wall value; however, it is believed that the chemical energy is low enough that the qualitative comparisons are valid, especially for the light engine load (2 bar). To further validate the results of this analysis, two BMEP power settings were chosen where unburned hydrocarbons and CO were insignificant.

As expected, Figure 10 shows that for both the 2 bar and 4 bar BMEP settings there is a decrease in heat lost through the wall due to the insulating qualities of the TBC. The remaining energy was split between the exhaust enthalpy and IMEP. Both power settings showed a significant increase in exhaust enthalpy, revealing the potential for an increase in power production with the implementation of a small turbocharger. The most important aspect in regards to fuel consumption and thermal efficiency, however, was the increase in IMEP when the TBC were applied. This increase in IMEP indicates that a higher percentage of fuel energy is being converted to mechanical work and therefore BSFC is reduced.

In order to understand the source of this extra mechanical work, an analysis of the **ignition delay** and **burn duration** was also conducted and is shown in Figure 11 with further explanation in Appendix A.6. The same points used for the first law analysis in Figure 10 were again used in this analysis. The ignition delay stayed nearly constant across both power variation and the addition of ceramic coatings; however, the burn duration of the fuel was slightly shorter with the TBC parts. Because of this, higher pressures were maintained longer through the power stroke, thereby increasing the PΔV work.

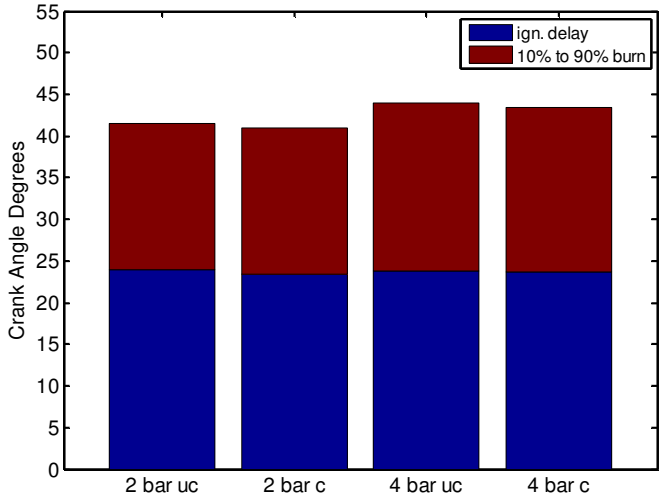

Figure 11: CAD of Ignition Delay and 10% to 90% Burn Completion

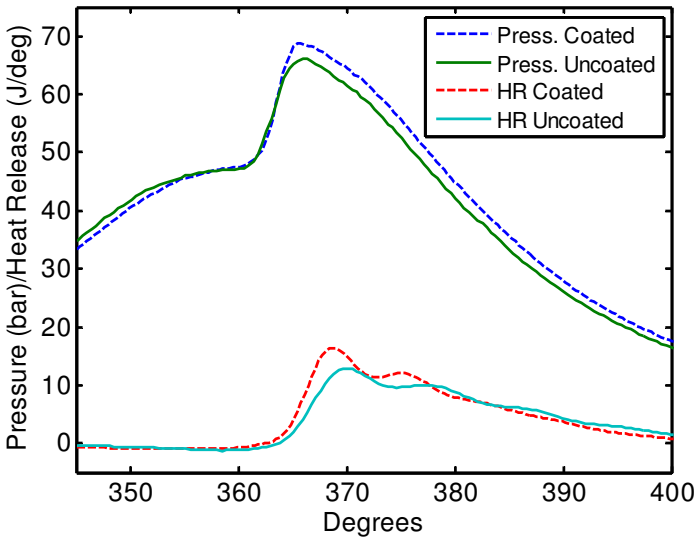

Figure 12: Pressure Trace and Instantaneous Heat Release Comparison of Optimized SOI CR21 TBC and Uncoated Parts with Heat Release Analysis

Further evidence of this conclusion is shown in Figure 12. Slight variations in compression pressures were noticed between coated and uncoated cases. This effect is believed to be due to slight changes in in-cylinder residual exhaust gas fraction with changed experimental conditions. The pressure traces of both the TBC and uncoated parts were essentially the same prior to the start of combustion (approximately TDC), therefore the temperatures at the start of combustion are believed to be very similar. This similarity in temperature explains the nearly constant value of ignition delay seen in Figure 11. Once the fuel started to burn however, the coated parts retained the heat of combustion and induced higher temperatures. This effect caused the fuel to burn more quickly, i.e. a higher heat release rate, which explains the reduced time required for 10-90% burn completion seen in Figure 11. The instantaneous rate of heat release remained higher for the coated engine until approximately 17 deg ATC, then became equal to that of the uncoated engine, which resulted in a consistently higher pressure trace for the TBC engine. The application of TBC to the engine resulted in the increased rate of fuel combustion, thereby creating higher pressures and more mechanical work.

The same set of analyses shown in Figures 10-12 were used to compare the performance of the TBC engine under varying CR and optimized SOI. A first law analysis is shown in Figure 13. As the CR was lowered, there was also a decrease in engine efficiency, which resulted in higher BSFC numbers at the lower CRs. CR21 (best BSFC point) is shown as having the lowest fraction of input fuel energy lost as exhaust enthalpy and the highest percentage lost to the walls, as the initial hypothesis of this work suggested. In this high CR configuration, the surface area to volume ratio plays a larger role in energy loss. The lower CRs do have less heat loss to the wall as the initial Ricardo WAVE simulation predicted but the exhaust energy has increased. A comparison of heat release analysis and pressure traces helps show why the lower CR points actually have worse BSFC.

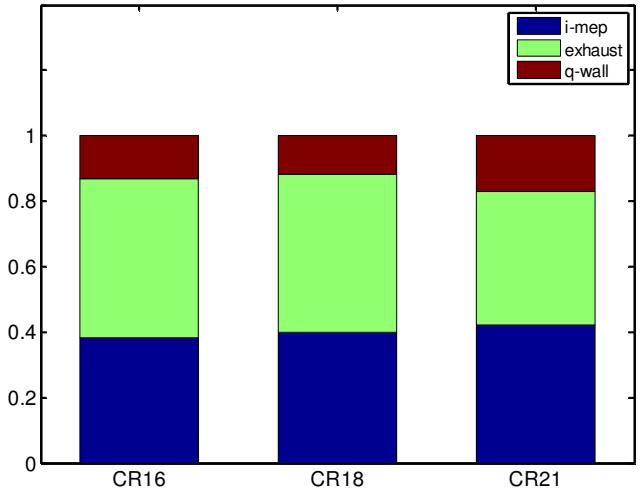

Figure 13: First Law Analysis of TBC, CRs 16, 18, and 21 with Optimized SOI at 2.5 bar BMEP

By analyzing the ignition delay and burn rate of the fuel with various CRs (Figure 14), it is evident that the lower CR cases have longer ignition delays and shorter 10-90% burn durations, but the overall SOI to 90% burn point is longer (total bar height). This is expected as cooler end of compression temperatures exist with less compression, thus longer times for kinetics to develop is expected. Longer ignition delays generally lead to more 'pre-mixing' of the diesel fuel and air, and thus shorter bulk burn durations (10-90% burn duration).

The issue with lower CRs in this engine is that combustion phasing could never be made as ideal as with the high CR21 configuration. Despite additional injection advance at CR16, it was difficult to advance combustion phasing due to the relatively cool environment at this low small diesel engine CR. It was seen that when injection timing was advanced earlier than the MBT SOI TBC CR16 case, the unburned hydrocarbon emissions approximately doubled. This fact reveals one of the causes of poor fuel conversion efficiency at this very advanced low CR condition. Only by changing the fuel to a very high cetane number (data not shown in this study) could combustion phasing be advanced with associated improvements in BSFC at CR16.

Representative in-cylinder pressure traces are shown to help further understanding this poor combustion phasing effect with lower CRs. Figure 15 shows in-cylinder pressure for CR16, 18 and 21 all with the MBT injection timings. It is evident that the PPLOC shifts later (less ideal) with lower CRs. This effect is what leads to a higher fraction of the fuel ending up as exhaust enthalpy (Figure 13) instead of piston work.

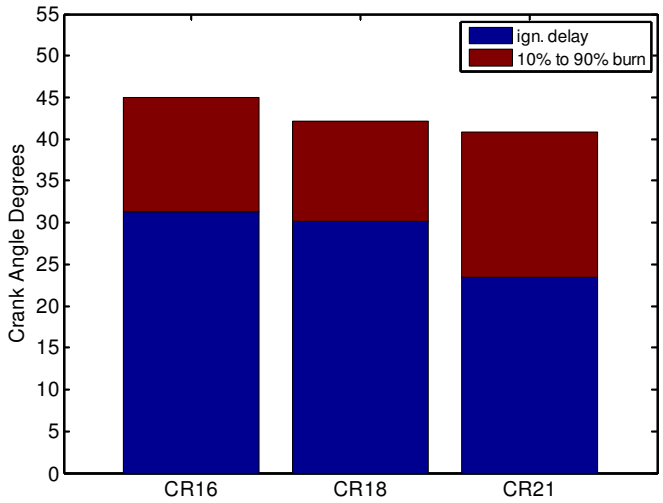

Figure 14: Ignition Delay and 10% to 90% Burn Completion for CRs 16, 18, and 21 with Optimized SOI at 2.5 bar BMEP

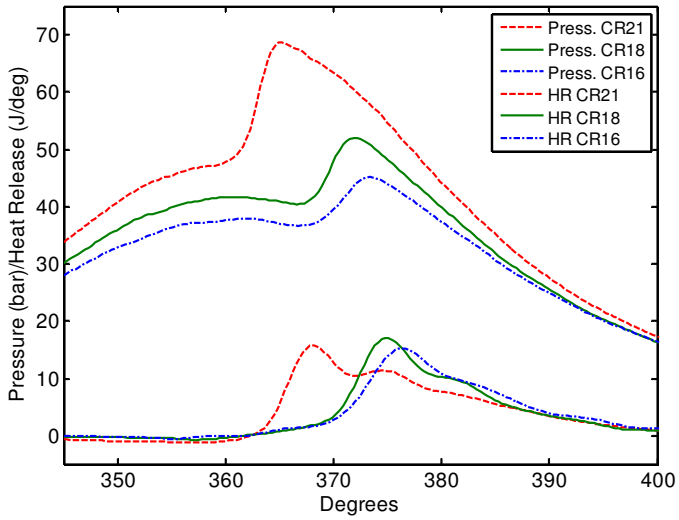

Figure 15: Pressure Trace and Instantaneous Heat Release Comparison of all TBC CRs at Optimized SOI

The first law energy analysis was completed when an investigation of the exhaust temperatures was conducted as is presented next. Exhaust temperatures dropped (or less fuel energy is left as exhaust enthalpy) as the engine operated more efficiently, as can be seen by comparing Figures 9 and 13. While exhaust temperatures do increase when the TBC were applied, this effect is believed principally due to less optimum combustion phasing with lower CRs as discussed above.

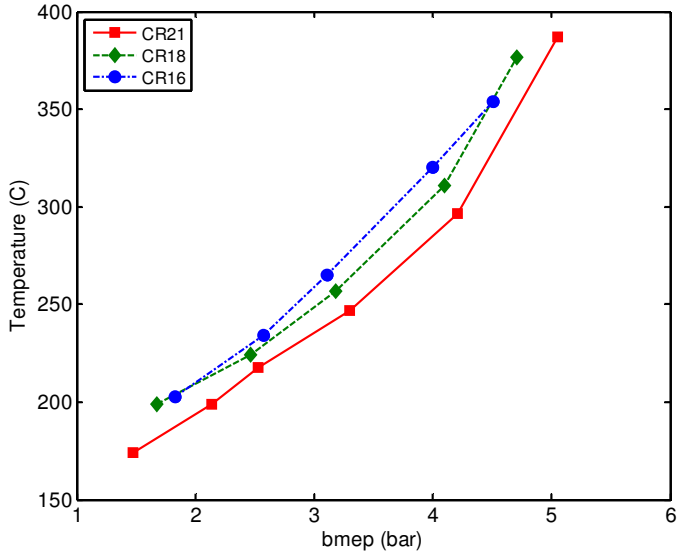

Figure 16: Exhaust Temperature at Optimized SOI for Each CR

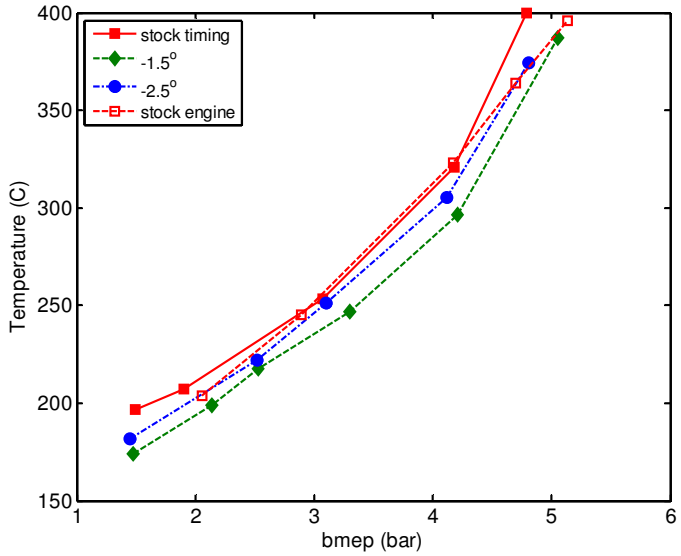

Figure 17: Exhaust Temperature at Various SOI Timings Compared to Stock Engine

This idea is further reinforced by comparing the exhaust temperatures of the SOI sweep that was discussed in regards to Figures 7 and 8. Again the lowest exhaust temperature coincides with the minimum BSFC. Lower exhaust temperatures indicated that a higher percentage of the fuel energy was converted into mechanical work and less was lost as sensible heat through the exhaust pipe. In the case of the stock SOI where the combustion was phased later, the fuel burned later and thus had less time to cool. In the case of the 2.5 degree advance, the pressure peaked too early, causing heat to prematurely release in the power stroke; however, the exhaust temperatures were lower due to this early burning of the fuel.

Little data were gathered from the common-rail injection system due to time constraints. The gross fuel consumption of the common-rail engine was very large due to the use of an oversized solenoid fuel injector that was designed for a per cylinder displacement of approximately ten times that of the Yanmar. Figure 18 shows a clear correlation of decreasing fuel consumption with increasing injection pressure even while the engine is being flooded with fuel by this large injector. The Sauter mean diameter trend, as described in Equation (1) earlier, was overlain on the fuel consumption data. By comparison, the engine efficiency is directly related to injection pressure, which is related to fuel droplet size.

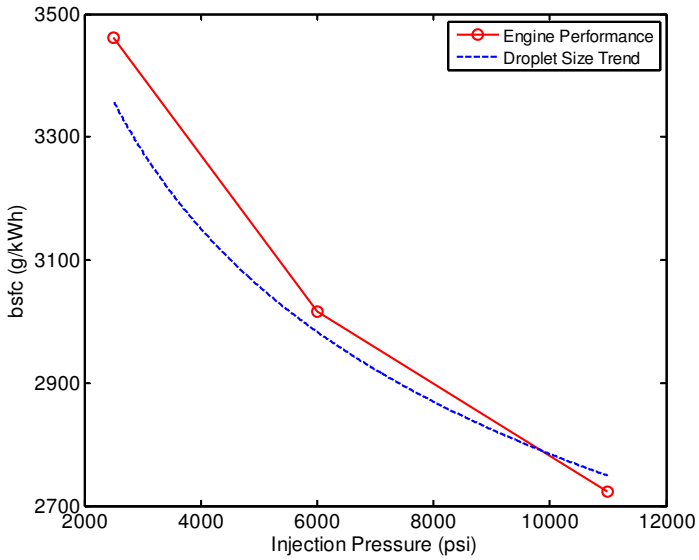

Figure 18: Fuel Consumption at Various Injection Pressures with Theoretical Droplet Size Trend Overlaid

Finally, a comparison of brake and indicated mean effective pressure was pursued as a check to ensure that frictional characteristics were not markedly different between all of the experimental cases. The BMEP was subtracted from the IMEP to yield the FMEP and these results are shown in Figure 19. It can be seen at this engine speed, 2750 rpm, and varying BMEP that FMEP is very constant along the bottom with a nominal value of 2 bar. There does not appear to be any significant difference between coated and uncoated parts, nor any significant difference with CR variations.

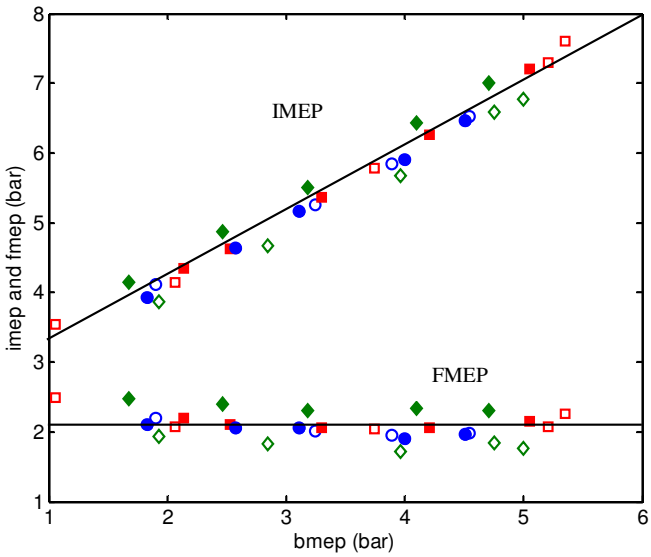

Figure 19: Trends in FMEP and IMEP for all CRs, TBC and Uncoated

4 Summary/Conclusions

Based on the test engine configurations described in this paper, the following conclusions are made:

With best-torque timing, the coated CR21 engine configuration showed decreased fuel consumption of approximately 10% in the low- to mid-load range while performance at maximum load was approximately the same relative to the uncoated stock engine. Reducing the CR, even with best-torque timing, resulted in increased fuel consumption at high loads; however, the low-load fuel consumption was very similar to the stock uncoated engine configuration. These results show that modest improvements in fuel consumption can be realized with TBC at CR21. They also suggest that similar fuel consumption may be achieved at reduced compression ratio for low- to mid-load conditions, allowing a smaller and lighter engine. The reduction in fuel consumption due to CR effects were not as significant as expected due to challenges appropriately phasing combustion with lower compression temperatures.

Simply adding TBC did not improve engine efficiency. Injection timing had to be set carefully to match the new operating environment in the engine, and small changes in injection timing resulted in large changes in fuel consumption. Improvements in BSFC were approximately 10% with timing optimization. Exhaust temperatures were also at a minimum with best-torque timing.

TBC had negligible effects on compression work; however, their insulating qualities allowed for hotter temperatures during combustion, which resulted in a slightly higher rate of heat release. Modest increases in heat release rate as a result of these TBC parts produced higher pressures and increased work output. Additionally, the TBC parts resulted in lower heat losses to the cylinder walls since the combustion took place when the majority of the combustion chamber was covered in the TBC.

Fuel injection pressure is directly related to engine efficiency. The fuel consumption drops as a function of the mean diameter of the fuel droplet. The significantly larger fuel consumption numbers seen with the adaptation of the common-rail system as compared to those of the stock engine could be reduced drastically by changing the fuel injector to one that is designed for a per cylinder displacement more comparable to the size of the Yanmar.

Based on these conclusions, the most efficient operating configuration for this engine would be at CR21 with the TBC at an optimized SOI timing. A corollary to this statement is that if reducing engine weight is more important than increasing its efficiency, a lighter engine with similar efficiency can be obtained at CR 18 or 16 with optimized SOI and TBC at low- to mid-load settings. Based on preliminary data from the common-rail system, the fuel consumption of the engine could be further reduced by fitting a properly sized injector to the engine.

5 References

[1] Alkidas A.C. 1999. Combustion-chamber crevices: the major source of engine-out hydrocarbon emissions under fully warmed conditions. *Progress in Energy and Combustion Science* 25:253–273.

[2] Çengel, Yunus and Michael A. Boles. *Thermodynamics an Engineering Approach*. 6th ed. Boston: McGraw-Hill, 2006.

[3] Challen, B. and Rodica Baranescu. *Diesel Engine Reference Book*. Elsevier: Oxford, 1999.

[4] Chun, K.M. and Heywood, J.B. 1987. 'Estimating Heat-Release and Mass-of-Mixture Burned from SI Engine Pressure Data', *Combustion Science and Technology* 54:133-143.

[5] Gatowski, J.A, Balles, E.N., Chun, K.M., Nelson, F.E., Ekchian, J.A. and Heywood, J.B. 1984. 'Heat Release Analysis of Engine Pressure Data', *SAE Technical Paper* #841359.

[6] Henein, N.A., and D.J. Patterson. *Emissions from Combustion Engines and Their Control.* Ann Arbor: Ann Arbor Science Publishers, 1972.

[7] Hejwowski T. and Weroński. 2002. The effect of thermal barrier coatings on diesel engine performance. *Vacuum* 65:427-432.

[8] Heywood, John B. *Internal Combustion Engine Fundamentals.* New York: McGraw-Hill, 1988.

[9] Judge, A.W. *High Speed Diesel Engines*. London: Chapman & Hall LTD., 1937.

[10] Parlak A., Yasar H., and Eldogan O. 2005. The effect of thermal barrier coating on a turbo-charged Diesel engine performance and exergy potential of the exhaust gas. *Energy Conversion and Management* 46:489-499.

[11] Parlak A., Yasar H., and Sahin B. 2003. Performance and exhaust emission characteristics of a lower compression ratio LHR Diesel engine. *Energy Conversion and Management* 44:163-175.

[12] Taymaz I. 2007. The effect of thermal barrier coatings on diesel engine performance. *Surface & Coatings Technology* 201:5249-5252

Appendix A: First Law Analysis

A first law analysis was conducted on the pressure data collected after each engine modification. This analysis treats the engine cycle as a closed system with one energy input from the fuel, Q_{fuel}, and three possible paths for energy to escape: the exhaust, $Q_{exhaust}$; the cylinder walls, Q_{wall}; or as mechanical work, $W_{P\Delta V}$. The generalized equation is shown below:

$$\Delta E = 0 = Q_{fuel} - Q_{exhaust} - Q_{wall} - W_{P\Delta V} \tag{1}$$

Expand each term in Equation (1) starting with the heat added by the fuel.

A.1 Q_{fuel}: Fuel Energy

The heat added by the fuel, calculated in Equation (2), is equal to the mass of the fuel injected multiplied by the lower heating value and the efficiency of combustion. The lower heating value is a chemical property of the fuel that can be found in a reference book [8]. Generally the combustion efficiency is very near unity, and therefore is sometimes neglected.

$$Q_{fuel} = \eta_{comb} m_{fuel} LHV_{fuel} \tag{2}$$

A.2 $Q_{exhaust}$: Exhaust Enthalpy

The heat lost to the exhaust, shown in Equation (4), is a simple measure of the exhaust gas enthalpy. The enthalpy of the gas was calculated by balancing the combustion reaction of Diesel fuel and air, which produced four gaseous products: carbon dioxide, water vapor, oxygen, and nitrogen. The enthalpy of each gas was calculated based on empirical formulas taken from a reference book, which expressed c_p as a function of temperature [2]. This relationship was integrated with respect to temperature to obtain enthalpy values as shown in Equation (3).

$$h_{exh} = \int c_p dT \tag{3}$$

The temperature used for enthalpy calculation was taken to be the theoretical temperature inside the cylinder the instant before the exhaust valve opened. The derivation of this temperature is shown in Equation (8). The thermocouple placed in the exhaust pipe gave qualitative trends in exhaust temperature; however, due to the rapid temperature drop of the exhaust gas as it flowed through the valve and expanded to the exhaust pipe, the theoretical temperature was used as a more standardized basis for comparison. The difference of the value of the enthalpy at this temperature and the enthalpy at room temperature was calculated and this value represented the enthalpy of the individual exhaust gases on a per mole basis.

$$Q_{exhaust} = \frac{h_{exh} m_{total}}{M_{exhaust}} \tag{4}$$

In order to combine the constituent gases according to their relative amounts, it was necessary to apply molar fractions to both the enthalpy calculations, not shown here, as well as the calculation of the molar mass of the exhaust gas as a whole, as seen in Equation (5). This molar mass was needed in order to relate the amount of exhaust gas to the mass of fuel injected. The total mass shown in Equation (4) refers to the mass of the fuel and the mass of the air in the cylinder at the time of combustion.

$$M_{exhaust} = Y_{CO_2} M_{CO_2} + Y_{H_2O} M_{H_2O} + Y_{O_2} M_{O_2} + Y_{N_2} M_{N_2} \quad (5)$$

.

It should be noted that the chemical energy of the exhaust is neglected in this calculation. Chemical energy shows up as unburned hydrocarbons and can be calculated with a detailed exhaust gas analysis. The exhaust gas analyzers used in this study were unreliable and therefore this data is unavailable. The error caused by neglecting the soot is assumed to be low.

A.3 Q_{wall}: Heat Loss to the Cylinder Walls

By far the most complex calculation in the energy balance is the amount of heat lost to the cylinder walls. In practical terms, this is the heat that is removed by the coolant, whether that is air or water. The general expression is shown in Equation (6). The total heat lost to the wall is a summation of the instantaneous heat transfer rate per **crank angle degree**. At each degree of crank shaft revolution the heat transfer coefficient, the area, and the temperature difference between the gases and the cylinder wall was reanalyzed.

$$Q_{wall} = C \int h(\theta) A(\theta) \Delta T(\theta) d\theta \quad (6)$$

The temperature difference shown in Equation (7), was defined as the theoretical mean temperature of the combustion gases and the cylinder wall with an assumed constant value of 450 ^{o}C. This value was not directly measured due to the complexity of placing a thermocouple close enough to the cylinder wall to gain an accurate measure of its temperature. The assumed constant value also simplified the calculation.

$$\Delta T(\theta) = T(\theta) - T_{\infty} \quad (7)$$

The instantaneous temperature in Equation (7) was calculated using the ideal gas law shown in Equation (8). This assumption was only valid during the closed portion of the engine cycle, which made the engine analysis less accurate. Once either valve opens, the mass of air in the cylinder changes rapidly, which makes the exact calculation of temperature nearly impossible. Another limitation of this model is that an initial temperature and mass of air must be assumed at the beginning of the closed portion of the cycle. The initial mass of air could be calculated from the volumetric flow rate of air; however, the instrumentation was unreliable, therefore a volumetric efficiency of 90% was assumed. Due to the limitations of calculating temperature, the heat transfer to the wall can only be calculated during the closed portion of the cycle. This introduces some error into the calculation; however, the highest temperatures and therefore the majority of the heat transfer occur during this stage of the engine's cycle. The pumping power

for the open part of the cycle remained nearly constant across all engine modifications; therefore while the absolute values of the energy balance have some error, the trends remain accurate.

$$T(\theta) = \frac{P(\theta)V(\theta)}{m(\theta)R(\theta)} \tag{8}$$

The instantaneous heat transfer coefficient was calculated using an empirical formula from Heywood's text [8] and is shown in Equation (9). The variable input to this equation must be in the units indicated in parenthesis for the exponent terms to work correctly. In this model, the heat transfer coefficient is a function of bore diameter, instantaneous pressure and temperature, and the piston's mean velocity multiplied by a constant as shown in Equation (10).

$$h(\theta) = 3.26B(m)^{-0.2}\, p(kPa)^{0.8} T(K)^{-0.55}\, w(m/s)^{0.8} \tag{9}$$

$$w = C_1 \overline{S}_P \tag{10}$$

The surface area of the cylinder is constantly changing and plays a critical role in this convective heat transfer model. An expression for the instantaneous area is shown in Equation (11). The top and bottom surfaces of the cylinder remain constant throughout the cycle with only the height of the cylinder changing. The face of the piston does have a bowl; however, the shape of the bowl was neglected and the piston face was assumed to be flat. The variable height of the cylinder is found by dividing the instantaneous volume, calculated in Equation (12), and dividing it by either the top or bottom circular areas.

$$A(\theta) = 2A_{top/bottom} + \frac{Vol(\theta)}{A_{top/bottom}} \pi d_{cyl} \tag{11}$$

The expression for instantaneous volume was taken from Heywood's text [8], and relates the length of the connecting rod, the compression ratio, and the stroke radius to volume for a given radial position and is shown in Equation (12). This calculation is important for not only the instantaneous heat transfer, but also the mechanical work and temperature calculations for the exhaust enthalpy.

$$V(\theta) = V_c(1 + 0.5(CR-1)(R+1-\cos(rad) - (R^2 - \sin(rad)^2)^{0.5})) \tag{12}$$

Further expanding the variable R in Equation (12) reveals that it is simply the ratio of the connecting rod length to the stroke radius.

$$R = \frac{L_{conrod}}{L_{strk\_rad}} \tag{13}$$

A.4 $W_{P\Delta V}$: Mechanical Work

The simplest calculation involved in the first law analysis was the integration of instantaneous pressure and volume values to yield mechanical work as expressed in Equation (14). The

instantaneous volume was calculated according to Equation (12). The pressure was derived from an in-cylinder pressure transducer. This transducer sends out a small charge when it undergoes a change in pressure. This charge is then converted to a voltage that is multiplied by a gain to yield the pressure in bar as shown in Equation (15). The gain for this system was 10. The pressure at intake valve close needs to be assumed while the noise in the pressure signal, due to mechanical vibration and pressure fluctuations from valve operation, is minimized by using a boxcar averaging technique. With this computational method, each pressure value is averaged with the next six datum points, resulting in a smoother pressure trace that is more favorable for accurate computation.

$$W = \oint P(\theta)V(\theta)d\theta \tag{14}$$

$$P(\theta) = Volt(\theta)K \tag{15}$$

A.5 Balancing the Energy

The heat lost to the exhaust, the mechanical work, and the heat added from the fuel are concrete values and can be calculated discretely. The general shape of the curve describing the instantaneous heat transfer to the wall is described by Equations (7-13); however, the magnitude of this curve is engine specific and therefore needs to be calculated at the end. A coefficient was placed in front of Equation (6) to represent a heat transfer multiplier. A lower multiplier indicates less heat loss to the walls with more energy directed to mechanical work and exhaust enthalpy. Because this coefficient is calculated based on the leftover energy from the fuel that did not go to the exhaust or to mechanical work, the energy is always balanced after the calculation is complete. The largest potential source for error is the amount of unburned hydrocarbons that are present in the exhaust. No attempt was made to integrate soot readings due to unreliable instrumentation. This error could be significant at high loads where soot levels tend to increase, thereby artificially driving up the heat loss to the wall.

A.6 Application

One of the most important uses for this first law analysis code is to calculate the heat release. From the heat release data, the burn duration and ignition delay can all be calculated. Equation (16) shows the expression used to calculate the heat release.

$$\delta Q_{ER} = \frac{k}{k-1} PdV + \frac{k}{k-1} VdP + \delta Q_{Wall} \tag{16}$$

In this expression, the differential heat released from the fuel is the sum of the three paths that the energy can take. The first term of pressure multiplied by a differential change in volume expresses the energy that goes to push the piston down and is by definition the mechanical work. The second path the fuel energy can take is to increase the pressure in the combustion chamber. The final term in this expression is the instantaneous heat lost to the cylinder walls. These

differential amounts of energy released are shown in Figures 12 and 15 along the bottom and have units of Joules/Crank Angle Degree. By summing these differential energy releases and knowing the total amount of energy the fuel contains, the ignition delay and burn duration can be calculated using their definition. The coefficient k is a ratio of the constant pressure specific heat, c_p, and the constant volume specific heat, c_v, and can be found by performing a complete differential analysis on the data; however, the explanation of this analysis is beyond the scope of the study and it can be safely assumed that k has a value of 1.3.

A.7 Implementation

In order to gain a better understanding, a version of this code was formulated and written by myself. Many issues regarding automated calculation proved difficult to resolve within the time frame spent developing and implementing this code. An engine data analysis code that was written by CAPT Len Hamilton that performs this analysis was implemented to save time. A comparison of the two codes' results showed that an error of less than 5% existed between them, which validated the theory behind both. Due to the high number of assumptions that were built into the code, this percent error can be taken to mean the results were identical. The following sections present the student developed code that consists of two function files and an input file, followed by the instructor developed code that consists of one file.

A.7.1 First Law Analysis Developed by MIDN 1/C Arment, USN

A.7.1.1 Exhaust Enthalpy

```
function [exh_energy]=exhaust(Texh,m_fuel,AF,m)

% Exhaust Enthalpy Calculation

Tinf=293;           %Sets the atmospheric temperature for a change in
                    %enthalpy comparison

%Texh=1050;
%m_fuel=0.0052;
%Combustion Balance
% C16H34 + AF*(O2+3.76N2)=b*CO2+c*H2O+d*N2+e*O2

%AF=211.62;
b=16;           %Balances the Combustion Reaction for a given Air Fuel Ratio
c=17;
e=AF-b-c/2;
d=3.76*AF;

%Variable Temperature Enthalpy for gas elements

%Integrate the cp equation to achieve...
%h(T)=w*T+x*T^2/2+y*T^3/3+z*T^4/4
```

```
%Nitrogen
P_N2= [-2.873e-9 0.8081e-5 -0.1571e-2 28.90 0];
h_N2=polyval(P_N2,Texh);
h_N2_inf=polyval(P_N2,Tinf);

%CO2
P_CO2= [7.469e-9 -3.501e-5 5.981e-2 22.26 0];
h_CO2=polyval(P_CO2,Texh);
h_CO2_inf=polyval(P_CO2,Tinf);

%H20

P_H2O= [-3.595e-9 1.055e-5 0.1923e-2 32.24 0];
h_H2O=polyval(P_H2O,Texh);
h_H2O_inf=polyval(P_H2O,Tinf);

%O2
P_O2= [1.312e-9 -0.7155e-5 1.520e-2 25.48 0];
h_O2=polyval(P_O2,Texh);
h_O2_inf=polyval(P_O2,Tinf);

%Exhaust Enthalpy

h_exh=b/(b+c+d+e)*(h_CO2-h_CO2_inf)+c/(b+c+d+e)*(h_H2O-h_H2O_inf)...
    +d/(b+c+d+e)*(h_N2-h_N2_inf)+e/(b+c+d+e)*(h_O2-h_O2_inf); %kJ/kmol
%Molar mass of the exhaust
Molar_mass=b/(b+c+d+e)*44+c/(b+c+d+e)*18+d/(b+c+d+e)*28+e/(b+c+d+e)*32;
m_tot=m_fuel+m*1000; %total mass in the cylinder
exh_energy=h_exh/Molar_mass*m_tot;
end
```

A.7.1.2 Energy Balance Code

```
function [engine_data] = PV2_fcn(deg, press,vol_fuel,t_fuel,AF)
eta_comb=0.999;                          %combustion efficiency
rc=16;                                 %compression ratio
global press_m t m_fuel
%Volume Calculation per Degree Crank Angle


rad=deg.*pi/180;                          %crank angle in radians
press_m=press.*10^5;                      %pressure in Pa
vd=pi*0.035^2*0.057;                     %displaced Volume (m^3)
vc=vd/(rc-1);                            %clearance volume (m^3)
R=0.092/.0285;                           %ratio conrod length/stroke radius
vol=vc.*(1+1/2*(rc-1)*(R+1-cos(rad)-(R.^2-sin(rad).^2).^(1/2))); %inst.
volume (m^3)
Work=trapz(vol,press_m);                    %Work (Joules)


%%
```

```
global m T



vel_avg=2750*0.114/60;          %average velocity in m/s
A1=2*pi*0.035^2;                %Area of the top and bottom of the piston
T_s=450;            %Assumed surface temperature of engine block in Kelvin
i=1;
T(i)=300;                       %initial temperature of incoming air
m=0.9*(101325*pi*0.035^2*0.057/(287*T(i))); %kg air in cyclinder initially
with 90% vol. eff
w=vel_avg.*2.28;                %Woschni coefficient
press_kPa=press_m./1000;        %In-cylinder pressure in kPa
for i=1:length(vol),
    T(i)=(press_m(i).*vol(i))/(m*287);
end

t=deg./(2750/60*360);           %time vector for one cycle
%%
%Energy In Q_in=m_fuel*HV_fuel

rho_fuel=0.840;                     %Density of Fuel (g/cc)
m_tot_fuel=vol_fuel*rho_fuel;       %total mass of the fuel consumed during
test (g)
num_cyc=t_fuel*2750/60/2;           %number of cycles
m_fuel=m_tot_fuel/num_cyc;          %g/combustion cycle
mole_fuel=m_fuel/226.34;            %moles of fuel
HV_fuel=43000;                      %Rough average of the values in Heywood
(J/g)
q_in=eta_comb.*m_fuel*HV_fuel;      %Theoretical heating value of the fuel

AFR=m*1000/m_fuel*226.34/29;        %Air/Fuel ratio
eta_th=Work./q_in;                  %Thermal Efficiency
%%
%Power & Torque
time_tot=max(t);                    %Length of cycle in seconds
HP=Work/time_tot/750;               %Indicated horsepower
omega=2750*pi/30;                   %engine speed in rad/sec
Torque=HP*750/omega/1.35913;        %Indicated torque

%%
%Mean Effective Pressure
Torque_m=Torque*1.35913;            %Torque in Nm
imep=Torque_m*4*pi/vd/100000;       %Indicated Mean Effective Pressure

%%
% Texh=mean(T(index_T_exh));
evo_ind= deg>490 & deg<491;         %Creates an index for exhaust valve
opening
T_evo_ind=T(evo_ind);               %Finds the temperature for EVO
Texh=mean(T_evo_ind);               %Averages T_exh for the data collection
cycle

exh_energy=exhaust(Texh,m_fuel,AF,m);%*mole_fuel;  %Finds the exhaust energy
                                    %using the exhaust function
```

```
%%
%Creates an instantaneous heat transfer coefficient based on the Woschni
%correlation, then calculates an instantaneous heat transfer rate assuming
%purely convective heat transfer with flat head and piston face
for i=1:length(vol);
    h_c(i)=3.26*0.07^(-0.2)*press_kPa(i).^(0.8)*T(i).^(-0.55).*w.^.8;
    q_conv(i)=(h_c(i).*A1.*(T(i)-T_s)+(T(i)-
T_s).*(2*pi*0.035*(vol(i)./(pi*.035^2)).*h_c(i))); %Basic convection
end

%Creates an array of instantaneous heat loss for the closed portion of the
%cycle
for i=1:length(deg)
    if deg(i)>230 && deg(i)<490
        q_loss_inst(i)=q_conv(i);
    else
        q_loss_inst(i)=0;
    end
end

q_loss=trapz(t,q_loss_inst);
%%
%Energy Balance

%Finds the heat transfer multiplier using an energy balance of Qin, exhaust
%energy, mechanical work, and heat loss
c=(q_in-Work-exh_energy)/q_loss;
q_loss=c*q_loss;
Diff=q_in-Work-q_loss-exh_energy;

%%
%Output
engine_data.Work = Work;
engine_data.q_loss = q_loss;
engine_data.deg = deg;
engine_data.Temp=T;
engine_data.q_in=q_in;
engine_data.HP=HP;
engine_data.Torque=Torque;
engine_data.vol=vol;
engine_data.h_multiplier=c;
engine_data.imep=imep;
engine_data.q_exh=exh_energy;
engine_data.energy_balance_error=Diff;
engine_data.Texh=Texh;
engine_data.evo=evo_ind;
engine_data.eta_th=eta_th;


figure(1)
plot(vol,press_m)                       %PV trace
xlabel('Volume (m^3)')
ylabel('Pressure (Pascal)')
title('PV trace')
```

A.7.1.3 Operating Code

```
clear all
close all

% Establish global variables
global deg press t_fuel vol_fuel AF

% Read in full data file
data = dlmread('54');

% Extract raw data of interest from large data file
voltage=data(:,1);                          %voltage of sensor
deg_raw=data(:,7);                          %crank angle degree

% Establish fuel flow data and AFR
t_fuel=49.4;                              %time of fuel consumption (s)
vol_fuel=10;                            %volume of fuel (cc)
AF=244.3876;%41.62*(226.34/29);

% Find indices corresponding to all TC locations
% cycle through the "deg_raw" vector, finding all the indices for which the
% following two conditions are met: CAD(i+1)-CAD(i) < 0 AND CAD(i+1) ~ 0.
% That should get only TC points.
j = 1;
for i=2:length(deg_raw)   % can't start at the very beginning of the vector
vector
    if (deg_raw(i)-deg_raw(i-1) < 0) & (deg_raw(i) < 1)
        TC(j) = i;
        j = j + 1;
    end
end

% Extract single cycles starting at overlap, convert pressure, scale, and
% analyze using PV function. To do this, we check every TC point and find
% the range of indices that corresponds to overlap to overlap.
j = 1;
for i=1:length(TC)-2                                    % "-2" ensures we can
extract last cycle is complete
    if (voltage(TC(i)) < voltage(TC(i+1)))              % if pressure at
current TC < pressure at next TC, then overlap

        % extract cycle
        first_rev_indices = [TC(i):(TC(i+1)-1)]';       % this is the range
corresponding to the first revolution, overlap TC to combustion TC
        sec_rev_indices = [TC(i+1):(TC(i+2)-1)]';       % this is the range
corresponding to the first revolution, combustion TC to next overlap TC
        volt_extract = voltage([first_rev_indices; sec_rev_indices]);
        deg = deg_raw(first_rev_indices);               % extracts
corresponding crank angle degrees for first rev
        deg(length(deg)+1:length(volt_extract)) = deg_raw(sec_rev_indices) +
360;    % here, we have to add 360 onto the second revolution
```

```
        % find location of BC, which is the best place to set 1 bar
        shift_value = mean(volt_extract(find((deg>175)&(deg<185))));    %
this line finds the part of the vector corresponding to 175-185 CAD and
averages it
        volt_extract_shift = volt_extract - shift_value;                %
adjusts the baseline to zero
        press = (volt_extract_shift .* 10) + 1;                         %
applies transfer function (volt to bar) and makes baseline 1 bar


        % analyze cycle using PV function
        [engine_data] = PV2_fcn(deg, press,vol_fuel,t_fuel,AF);

        % store cycle data
        imep(j) = engine_data.imep;  % note that index is different than i,
which will skip values
        q_loss(j)=engine_data.q_loss
        q_in(j)=engine_data.q_in;
        eta_th(j)=engine_data.eta_th;
        h_multiplier(j)=engine_data.h_multiplier;
        Work(j)=engine_data.Work;

        % ... other metrics

        j = j + 1;
    end
end
%Output mean values of given parameters over the data collection cycle
imep=mean(imep(2:j-2))
q_loss_m=mean(q_loss(2:j-2))
q_in=mean(q_in(2:j-2))
eta_th=mean(eta_th(2:j-2))
h_multiplier=mean(h_multiplier(2:j-2))
Work=mean(Work(2:j-2))




%deg_index=1:length(deg_raw);            %length of degree vector
%deg_step_size=720/length(deg_raw);      %equally divides the degrees vector
into steps
%deg=deg_index.*deg_step_size;           %720 degree vector
%press_raw=voltage*10;                   %uncorrected pressure
%min_press=abs(min(press_raw));
%for i=1:length(press_raw)
%    press_correct(i)=press_raw(i)+min_press+0.3;  %corrected pressure
%end
%press=press_correct;
```

A.7.2 First Law Analysis Developed by CAPT Hamilton, USN

```
%This program analyzes diesel data for yanmar engine
%L.J. Hamilton 4-15-2008


% data column 1: date
% data column 2: time
% data column 3 - cylinder pressure (p) 10 bar/volt
% data column 4 - top dead center (tdc) hi to low is TDC
% data column 5 - MAF (currently inop)
clear all
format compact
close all

num_start = input('Please enter file name start number:');
num_finish = input('Please enter last file name number:');

for findex = num_start:num_finish
    filename = strcat('a', num2str(findex));  %,'.dat'

    disp(sprintf('Opening and analyzing %s.', filename));

data = load(filename);



p = data(:,1); %(volts)
tdc = data(:,7);
%MAF = data(:,3); %(volts)


n = size(p);

start = 1; %used to initialize graphing window

%engine parameters
b = 0.07; %bore (m)
s = 0.057;  %stroke (m)
l = 0.095; %con rod length (m) (this is a guess)
pcal = 10;   %10 bar per volt

%inputs to be changed for various load conditions
voleff = 0.85; %volumetric efficiency
RPM = 2750;
fueltime = 46.1; %fuel burn time (sec) from data sheet yx10 = 49.4 sec for
10cc

r = 287; %gas constant
spbar = 2*RPM*s; %mean piston speed (m/s)
w = 2.28*spbar; %woschni velocity
twall = 450; %K this is a guess-timate
gam = 1.26; %gamma
```

```
%************************must be changed for each
run************************
rc = 21;  %compression ratio
tin = 293; %K
ccfuel = 10; %quantity of fuel burned (cc)

mg = (ccfuel*60*840*2)/RPM/fueltime; %mg of fuel injected. 840 mg/cc d2, 750
mg/cc FT, RPM/2 is shots per min
kgfuel = mg/1e6; %kg of fuel injected
etotrel = kgfuel*42.5e6 %J  max available energy (LHV d2=42.5,
FT=43.7,C7=44.6 MJ/kg)
c1 = 0.07; %must be varied to ensure realistic energy release plot and
combeff <= 0.95

%engine calcs
piar = pi*b2/4; %piston area (m2)
a =s/2;
vd = s*piar;  %diplacement volume (m3)
vc = vd/(rc-1); %clearance volume (m3)

%Find the index locations for tdc (power)
iitdc = 0;
itdc = 1;
for i = 2:n(1,1);
    if tdc(i-1)-tdc(i)>50  %needs to be 2.5 for starts, 2.0 for ss.
        if p(i)>2  %this eliminates tdc at beginning of intake stroke
            if i-iitdc(itdc)>10
                itdc=itdc+1;
                iitdc(itdc)=i-1;
            else
            end

        else
        end
    else
    end
end
numcyc = length(iitdc);
%we now have  a list of all tdc locations preceding power stroke

iitdc_temp = iitdc(2:numcyc);
clear iitdc;
iitdc = iitdc_temp;

%determine cycle length
itdc = 1;

% for itdc = 2:numcyc-1;
for itdc = 3:33;

        iratio(itdc) = (iitdc(itdc)-iitdc(itdc-1))/720;  %this is in
samples/degree
```

```
        iibcc(itdc-1) = iitdc(itdc-1) - round(iratio(itdc)*180);  %this marks
bottom center for compression
        iibce(itdc-1) = iitdc(itdc-1) + round(iratio(itdc)*180);  %this marks
bottom center for compression
        iiqend(itdc-1) = iitdc(itdc-1) + round(iratio(itdc)*150);  %this
marks end of useful burn (100 deg past tdc)
        pbcc = (p(iibcc(itdc-1)-2)+ p(iibcc(itdc-1))+ p(iibcc(itdc-1)+2))/3;

        pmap(itdc-1) = 1;   %manifold pressure in bar

        ivol1 = [iibcc(itdc-1):1:iibce(itdc-1)]'; %indices from bcc to bce
        ivol2 = [iibcc(itdc-1)+1:1:iibce(itdc-1)+1]';
        crankrad1 = (ivol1-ones(length(ivol1),1)*iibcc(itdc-
1))*pi/iratio(itdc)/180; %crank angle in radians where bcc = 0
        crankrad2 = (ivol2-ones(length(ivol2),1)*iibcc(itdc-
1))*pi/iratio(itdc)/180;
        tsec1 = crankrad1./30/pi;  %this is elapsed time between data samples
        tsec2 = crankrad2./30/pi;
        deltime = tsec2-tsec1;
        s1 = a*cos(crankrad1+ones(length(ivol1),1)*pi)+sqrt(l2-
a2*(sin(crankrad1+pi)).^2);
        s2 = a*cos(crankrad2+ones(length(ivol2),1)*pi)+sqrt(l2-
a2*(sin(crankrad2+pi)).^2);
        v1 = vc*ones(length(ivol1),1) + piar*((l+a)*ones(length(ivol1),1)-
s1);
        v2 = vc*ones(length(ivol2),1) + piar*((l+a)*ones(length(ivol2),1)-
s2); %volume in m3
        delv = v2-v1;
        p1 = (p(ivol1)-ones(length(ivol1),1)*pbcc)*pcal +
ones(length(ivol1),1); %cylinder pressure in bar
        p2 = (p(ivol2)-ones(length(ivol2),1)*pbcc)*pcal +
ones(length(ivol1),1); %cylinder pressure in bar

        delp = p2-p1;

        cylmass(itdc-1) = voleff*pmap(itdc-1)*vd*101325/r/tin;  %kg, assumes
map = 1 bar
        tincyl = p2.*v2.*100000/r/cylmass(itdc-1);
        pmot = (pmap(itdc-1)*((vd+vc)./v2)).^1.33;  %note the use of decimals
for future use.  freaking painful!
        ww = w*ones(length(ivol2),1) + 0.00324*300*(p2-pmot)/pmap(itdc-1);
%where did 0.00324 come from?

        %Blowby loss:
       c2 = 0.00; %vary this constant until qrel = 0 for motoring cases
       blowvol=c2*(p1-p1(1)).^1.7;  %assume blowby volume is directly
proportional to cylinder pressure
       blowloss = blowvol; %energy lost to blowby, J

        ahc = c1*1.637*(p2*100).^0.8 + (tincyl.^-0.55).*ww.^0.8; %heat
transfer coefficient
        areacc = 2*piar*ones(length(ivol2),1)+pi*2*b*v2./piar;  %m2
        qdotwall = ahc.*areacc.*(tincyl - twall); %J/s
        qwallsum = cumsum(qdotwall).*deltime; %J
```

```
        qnet = p2.*100000.*delv.*(gam/(gam-1)); %not sure where this came
from?

        pdv = p2.*100000.*delv;
        wpdv = cumsum(pdv); %J

        imepg(itdc-1) = dot(p1,piar*(s1-s2)/vd); %mean effective pressure

        cp = gam*1.0*ones(length(tincyl),1);  %specific heat capacity for air

        egas = 1000*cylmass(itdc-1)*cp.*(tincyl-
tincyl(1).*ones(length(tincyl),1)); %enthalpy of air (J)
        deltat = tincyl-tincyl(1).*ones(length(tincyl),1);

        crank20 = crankrad2*180/pi-180-0.*ones(length(crankrad2),1);
        [c0, i0] = min(abs(crank20)); %finds the index for 0 degree ATDC
        crank150 = crankrad2*180/pi-180-150.*ones(length(crankrad2),1);
        [c150, i150] = min(abs(crank150)); %finds the index for 150 degree
ATDC

        qrel = egas + wpdv + qwallsum + blowloss;  %energy balance (1st law)

        wnet(itdc-1) = wpdv(i150); %net work (J)
        qout(itdc-1) = qrel(i150);
        enth(itdc-1) = egas(i150);
        qloss(itdc-1)= qwallsum(i150);


      %find injector pulse start
%         injseg = ijpos([iibcc(itdc-1):1:iibce(itdc-1)]);
%         [maxinj(itdc-1),imaxinj(itdc-1)]= max(injseg);
%         injstart(itdc-1) = imaxinj(itdc-1)/iratio(itdc)-3;  %start of
injector pulse in degrees after bcc (-3 degrees correction)

      %this section "smoothes" heat released data to provide more accurate
5%,10% and 90% burn results
        [B,A]=cheby1(3,2,.1);
        qrelfilt1 = filter(B,A,qrel);
        qrelfilt = 1.0*qrelfilt1;
        %qrelfilt2 = qrelfilt([imaxinj(itdc-1):1:(iiqend(itdc-1)-iibcc(itdc-
1))]);
        qrelfilt3 = (qrelfilt1([1:1:length(ivol1)-
2])+qrelfilt1([2:1:length(ivol1)-1])+qrelfilt1([3:1:length(ivol1)]))/3;
% rate of heat release calculations:
rawdelqrel=(qrelfilt3([2:1:length(ivol1)-2])-qrelfilt3([1:1:length(ivol1)-
3])); %provides data for rohr
[B,A]=cheby1(1,1,.01);
delqrel = filter(B,A,rawdelqrel);
%if imaxinj(itdc-1)<=(iiqend(itdc-1)-iibcc(itdc-1))  %added for odd case when
max inj occurs very late.
 %       [maxqrel,imaxqrel(itdc-1)] = max(qrelfilt2);
%        imaxqrel(itdc-1) = imaxqrel(itdc-1)+imaxinj(itdc-1);

%else [maxqrel,imaxqrel(itdc-1)] = max(qrelfilt1);
    [maxqrel,imaxqrel(itdc-1)] = max(qrelfilt1);
```

```
    imaxinj(itdc-1)=1;
    qrelfilt2=qrelfilt1;
%end
        combeff(itdc-1) = 100*maxqrel/etotrel;

     %Finding crank angle when 5% of burn complete
        qrelfilt4 = qrelfilt([imaxinj(itdc-1):1:imaxqrel(itdc-1)]);
        fivenq = qrelfilt4 - 0.05*maxqrel.*ones(length(qrelfilt4),1);  %this
produces a vector with zero at 5% of qrel
        [q05, i05]= min(abs(fivenq)); %produces index for 5% of qrel
        crank05(itdc-1) = crankrad2(i05+imaxinj(itdc-1))*180/pi-180; %crank
angle for 5% burn


     %Finding crank angle when 20% of burn complete
        tenq = qrelfilt4 - 0.2*maxqrel.*ones(length(qrelfilt4),1);  %this
produces a vector with zero at 10% of qrel
        [q10, i10]= min(abs(tenq)); %produces index for 10% of qrel
        crank10(itdc-1) = crankrad2(i10+imaxinj(itdc-1))*180/pi-180; %crank
angle for 10% burn

     %Finding crank angle when 90% of burn complete
        ninetyq = qrelfilt4 - 0.9*maxqrel.*ones(length(qrelfilt4),1);  %this
produces a vector with zero at 90% of qrel
        [q90, i90]= min(abs(ninetyq));  %produces index for 90% of qrel
        crank90(itdc-1) = crankrad2(i90+imaxinj(itdc-1))*180/pi-180; %crank
angle for 90% burn




        [peakp(itdc-1), ipeak(itdc-1)] = max(p1); %finds location of max
pressure
        %convert ipeak to degrees after bcc
        ipeakdeg(itdc-1) = ipeak(itdc-1)/iratio(itdc);


        %analyze pressure rise

        diff = qrel - qwallsum;
        diffseg = diff([(iitdc(itdc-1)-iibcc(itdc-1)-
round(iratio(itdc)*20)):1:(iibce(itdc-1)-iibcc(itdc-1))]); %evaluate diff
from 20 btc to bce
        [mindiff(itdc-1),irise(itdc-1)]= min(abs(diffseg));  %index for min
diff (which is beginning of burn-induced pressure rise)
        irisestart(itdc-1) = irise(itdc-1)/iratio(itdc); %start of cylinder
pressure rise rel to TDC (deg)
        irisestart2(itdc-1) = irise(itdc-1)+(iitdc(itdc-1)-iibcc(itdc-1)-
round(iratio(itdc)*20)); %start of cylinder pressure rise rel to BCC (data)
        irisebcc(itdc-1)= irise(itdc-1) + iitdc(itdc-1)-iibcc(itdc-1); %start
of cylinder press rise rel to BCC (data points)
        irisebcc2(itdc-1)= i10 + iitdc(itdc-1)-iibcc(itdc-1); %start of
cylinder press rise rel to BCC (data points)
```

```
        %prise(itdc-1) = p1(irisebcc2(itdc-1));  %pressure at beginning of
rise (bar)
        %prise(itdc-1) = p1(irisestart2(itdc-1));  %pressure at beginning of
rise (bar)
        prise(itdc-1) = p1(i10-round(iratio(itdc)*3));  %pressure at
beginning of rise (bar)
        pressrise(itdc-1) = peakp(itdc-1) - prise(itdc-1); %peak - pressure
at beginning of pressure rise
        pressgrad(itdc-1) = pressrise(itdc-1)*iratio(itdc)/(ipeak(itdc-1)-
i10); %pressure gradient (bar/deg)

       % igndelay(itdc-1) = 180 + crank05(itdc-1)- injstart(itdc-1);
%ignition delay based on 5% burn(deg)



        viewstart = 1;
        viewend = 359;
   volstart(itdc-1) = round(iratio(itdc)*viewstart);  %this marks start of
expanded view
   volend(itdc-1)= round(iratio(itdc)*viewend); %this marks the end of
expanded view

   d = (180/pi)*crankrad1([volstart(itdc-1):volend(itdc-1)])';  %this is
graph view in degrees
   press = p1([volstart(itdc-1):volend(itdc-1)])'; %index relative to
volstart
   rohr=iratio(itdc)*delqrel([volstart(itdc-1):volend(itdc-1)])';  %rate of
heat release (J/sample) index rel to volstart
%    brint=rohr([imaxinj(itdc-1)-volstart(itdc-1):(imaxinj(itdc-1)-
volstart(itdc-1)+iratio(itdc)*10)]); %creates a subset of rohr to seek
premixed peak

%   brint=rohr([imaxinj(itdc-1)-volstart(itdc-1):(imaxinj(itdc-1)-
volstart(itdc-1)+iratio(itdc)*10)]); %creates a subset of rohr to seek
premixed peak
%   [maxrohr(itdc-1),imaxrohr(itdc-1)]= max(brint); %index relative to
imaxinj
%    imaxrohr(itdc-1)=imaxrohr(itdc-1)+ imaxinj(itdc-1); %index relative to
bcc
%    iburndiv(itdc-1)=imaxrohr(itdc-1)+(imaxrohr(itdc-1)-i05-imaxinj(itdc-
1)); %index relative to bcc
%    burnratio(itdc-1)=qrel(iburndiv(itdc-1))/maxqrel;
   %cycle plots

   figure(itdc-1)
   clf
subplot(2,1,1)

   plot(d-180,press)
   grid
   hold on
 %  plot(injstart(itdc-1)-180,3,'r*');
  % plot(ipeakdeg(itdc-1)-180,50,'rd');
 %  plot(crank10(itdc-1)-3,3,'r*');
   axis([viewstart-180,viewend-180,-5,100])
```

```
   hold off
   text(-140,64,['peak press = ',num2str(peakp(itdc-1)),' bar'])
   text(-140,56,['peak press at ',num2str(ipeakdeg(itdc-1)-180),' deg ATC'])
   text(-140,48,['pressure jump = ',num2str(pressrise(itdc-1)),' bar'])
   text(-140,40,['pressure gradient = ',num2str(pressgrad(itdc-1)),'
bar/deg'])
   text(-140,32,['pressure at rise = ',num2str(prise(itdc-1)),' bar'])
%   text(-140,18,['injector adv = ',num2str(180-injstart(itdc-1)),' deg
BTC'])
%   text(-140,12,['ignition delay = ',num2str(igndelay(itdc-1)),' deg'])
   title([num2str(char(filename)),' cycle',num2str(itdc-1)])
   xlabel('crankangle(deg rel to TDC)');ylabel('cylinder pressure (bar)')

subplot(2,1,2)
    plot(d-180,tincyl([volstart(itdc-1):volend(itdc-1)]),'r-');

   grid
 hold on
 %   plot(d-180,10*rohr,'r');
 %   plot(crank05(itdc-1),-300,'g*');
 %   plot(crank10(itdc-1),-300,'b*');
 %   plot(crank90(itdc-1),-300,'b*');
%    plot(imaxrohr(itdc-1)/iratio(itdc)-180,-200,'g*');
%    plot(iburndiv(itdc-1)/iratio(itdc)-180,-200,'r*');
    plot(d-180,qrel([volstart(itdc-1):volend(itdc-1)]),'b');
    plot(d-180,qwallsum([volstart(itdc-1):volend(itdc-1)]),'k-');
    plot(d-180,wpdv([volstart(itdc-1):volend(itdc-1)]),'g-.');
 %   plot(d-180,qrelfilt1([volstart(itdc-1):volend(itdc-1)]),'c--');

   axis([viewstart-180,viewend-180,-500,2000])
   text(-120,1300,['crank angle for 90% of qrel =',num2str(crank90(itdc-1))])
   text(-120,900,['crank angle for 20% of qrel =',num2str(crank10(itdc-1))])
   text(-120,1700,['combustion efficiency =',num2str(combeff(itdc-1))])
   text(50,1700,['enthalpy change =',num2str(enth(itdc-1)),' J'])
   text(50,1300,['thermal efficiency =',num2str(mean(100*wnet./etotrel)),'
%'])
   text(50,900,['energy released =',num2str(qout(itdc-1)),' J'])
   text(50,400,['heat lost to wall =',num2str(qloss(itdc-1)),' J'])
   text(50,-100,['net work =',num2str(wnet(itdc-1)),' J'])
   legend('Tgas(K)','energy released(J)','heat
lost(J)','work(J)','Location','Southwest');

   xlabel('crankangle(deg rel to TDC)');ylabel('Energy(J),Tgas(K)')
hold off

   orient tall
   print -depsc  cycleplot  %rename to match first part of data file

   if itdc ==8;
%        fid = fopen('dataset1.txt','wt');
       dataset = [d'-180,rohr',press'];
% fprintf(fid,'%7.2f %7.2f %7.2f\n',dataset);
% fclose(fid);
xlswrite('results.xls',dataset,num2str(findex));
   else
   end
```

```
 end



figure(numcyc+1)
clf
subplot(3,1,1)
plot([1:1:itdc-1],imepg(1:1:itdc-1),'o-')
hold on
grid
text(2,max(imepg)+5,['average imep = ',num2str(mean(imepg)),' bar'])
%text(15,max(imepg)+5,['standard dev = ',num2str(std(imepg)),' bar'])
plot([1:1:itdc-1],pressrise(1:1:itdc-1),'+-')
text(2,min(pressrise) + 15,['average pressure jump =
',num2str(mean(pressrise)),' bar'])
%text(15,min(pressrise) + 5,['standard dev = ',num2str(std(pressrise)),'
bar'])
text(2,max(pressrise) + 20,['average pressure gradient =
',num2str(mean(pressgrad)),' bar/deg'])
%text(15,max(pressrise) + 15,['standard dev = ',num2str(std(pressgrad)),'
bar/deg'])
plot([1:1:itdc-1],peakp(1:1:itdc-1),'^-')
text(2,max(peakp) + 5,['average peak pressure = ',num2str(mean(peakp)),'
bar'])
%text(15,max(peakp) + 5,['standard dev = ',num2str(std(peakp)),' bar'])
hold off

axis([1,numcyc-1,0,max(peakp)+10])
xlabel('cycle #');ylabel('imep (bar)')
title(num2str(char(filename)))

subplot(3,1,2)
plot([1:1:itdc-1],crank10(1:1:itdc-1),'o-')
hold on
text(2,min(crank10) + 10,['average angle for 20% burn =
',num2str(mean(crank10)),' deg'])
plot([1:1:itdc-1],crank90(1:1:itdc-1),'d-')
text(2,max(crank90) + 5,['average angle for 90% burn =
',num2str(mean(crank90)),' deg'])
% plot([1:1:itdc-1],injstart(1:1:itdc-1)-180,'*-')
% text(2,min(injstart-180) + 5,['average injector advance =
',num2str(mean(injstart-180)),' deg'])
plot([1:1:itdc-1],ipeakdeg(1:1:itdc-1)-180,'^-')
text(2,max(ipeakdeg-180) + 25,['average angle max pressure =
',num2str(mean(ipeakdeg-180)),' deg'])
%text(2,max(crank90) + 15,['average ignition delay =
',num2str(mean(igndelay)),' deg'])
axis([1,numcyc-1,-20,max(crank90)+20])
grid
xlabel('cycle #');ylabel('crank angle (deg ATDC)')
hold off

subplot(3,1,3)
plot([1:1:itdc-1],combeff(1:1:itdc-1),'o-')
hold on
xlabel('cycle #');ylabel('efficiency(%)')
```

```
axis([1,numcyc-1,0,160])
text(2,80,['avg combeff = ',num2str(mean(combeff)),'%'])
text(80,80,['C1 = ',num2str(c1)])
plot([1:1:itdc-1],100*wnet(1:1:itdc-1)./etotrel,'d-')
%text(2,27,['thermal efficiency'])
text(2,30,['average thermal efficiency =
',num2str(mean(100*wnet./etotrel)),'%'])
%text(15,47,['compression ratio = ',num2str(rc)])
hold off
grid
orient tall
print -depsc  summary  %rename to match first part of data file
%print

% figure(numcyc+2)
% clf
% plot([1:1:itdc-1],burnratio(1:1:itdc-1),'o-')
% axis([1,numcyc-1,0,1])
% xlabel('cycle #');ylabel('burn ratio')
% title([num2str(char(filename))])
%print

% fid = fopen('results.txt','a');
% %fprintf(fid,'%6.2f %6.2f %6.2f %6.2f %6.2f %6.2f %6.2f %6.2f %6.2f %6.2f
%6.2f %6.2f %6.2f\n',fueltime,rc,mean(180-
injstart),mean(crank10),mean(ipeakdeg-
180),mean(igndelay),mean(crank90),mean(imepg),mean(pressrise),mean(peakp),max
(qwallsum),mean(100*wnet./etotrel),mean(burnratio));
% fprintf(fid,'%6.2f %6.2f %6.2f %6.2f %6.2f %6.2f %6.2f %6.2f %6.2f
%6.2f\n',fueltime,rc,mean(180-
injstart),mean(igndelay),mean(imepg),mean(peakp),mean(ipeakdeg-
180),mean(crank90),mean(100*wnet./etotrel),mean(burnratio));
% fclose(fid);
end
mean(combeff)
mean(qloss)
```

Appendix B: General Matlab Code

B.1 BSFC vs. BMEP

```
clear all
close all

%Creates a plot of bsfc vs. bmep. This plot is used several times
%throughout the report, only the variables are changed

Vd=0.00021;                          %Displaced engine volume
data=xlsread('rc21_phasing.xls');    %Read in the data
%following calculations are redundant
t_s=data(1:4,1)*1.35581795;          %Measured Torque
bmep_s=t_s*4*pi/Vd/100000;           %Convert Torque to bmep
bsfc_s=data(1:4,2);                  %Measured bsfc

t_15=data(1:5,3)*1.35581795;
bmep_15=t_15*4*pi/Vd/100000;
bsfc_15=data(1:5,4);

t_25=data(1:4,5)*1.35581795;
bmep_25=t_25*4*pi/Vd/100000;
bsfc_25=data(1:4,6);

%Scatter plot of the data
plot(bmep_s,bsfc_s,'rs-',bmep_15,bsfc_15,'gd--',bmep_25,bsfc_25,'bo-.')
xlabel('bmep (bar)')
ylabel('bsfc (g/kWh)')
legend('stock','-1.5^o','-2.5^o')
axis([1 6 300 550])                  %Sets the axis limits


%Compares cr21 at three different SOI
```

B.2 IMEP and FMEP vs. BMEP

```
clear all
close all

%Produces a scatter plot comparison of imep and fmep vs. bmep

data=xlsread('gmep_c_vs_uc.xls');
Vd=0.00021;                          %Displaced Volume of the engine
t21uc=data(1:5,1)*1.35581795;        %Measured Torque
bmep_21uc=t21uc*4*pi/Vd/100000;      %Calculated bmep
```

```
gmep21uc=data(1:5,2);                %gmep calculated from in-cylinder
pressure
fmep_21uc=gmep21uc-bmep_21uc;        %fmep, (gmep-bmep)

t18uc=data(1:5,3)*1.35581795;
bmep_18uc=t18uc*4*pi/Vd/100000;
gmep18uc=data(1:5,4);
fmep_18uc=gmep18uc-bmep_18uc;

t16uc=data(1:4,5)*1.35581795;
bmep_16uc=t16uc*4*pi/Vd/100000;
gmep16uc=data(1:4,6);
fmep_16uc=gmep16uc-bmep_16uc;

t21c=data(1:5,7)*1.35581795;
bmep_21c=t21c*4*pi/Vd/100000;
gmep21c=data(1:5,8);
fmep_21c=gmep21c-bmep_21c;

t18c=data(1:5,9)*1.35581795;
bmep_18c=t18c*4*pi/Vd/100000;
gmep18c=data(1:5,10);
fmep_18c=gmep18c-bmep_18c;

t16c=data(1:5,11)*1.35581795;
bmep_16c=t16c*4*pi/Vd/100000;
gmep16c=data(1:5,12);
fmep_16c=gmep16c-bmep_16c;

%Creates a scatter plot of all data either imported or calculated above
plot(bmep_21uc,gmep21uc,'rs',bmep_18uc,gmep18uc,'gd',bmep_16uc,gmep16uc,'bo'.
..
    ,bmep_21c,gmep21c,'rs',bmep_18c,gmep18c,'gd',bmep_16c,gmep16c,'bo',...
    bmep_21uc,fmep_21uc,'rs',bmep_18uc,fmep_18uc,'gd',bmep_16uc,fmep_16uc...

,'bo',bmep_21c,fmep_21c,'rs',bmep_18c,fmep_18c,'gd',bmep_16c,fmep_16c,'bo')
xlabel('bmep (bar)');
ylabel('imep and fmep (bar)')
```

B.3 Pressure Trace and HR from Data Output from First Law Analysis

```
clear all
close all

data=xlsread('yanmar_2bar_cycle_pressure_comparison.xls');

%CAD = Crank Angle Degrees
%HR = Heat Release (J/deg)
deg_c=data(:,5)+360;     %CAD output of the crank shaft encoder Coated Parts
deg_uc=data(:,1)+360;    %CAD output of the crank shaft encoder Uncoated Parts
press_c=data(:,7);       %Pressure output of the first law code Coated
press_uc=data(:,3);      %Pressure output of the first law code Uncoated
```

```
hr_c=data(:,6);          %Instantaneous HR of Coated Parts
hr_uc=data(:,2);         %Instantaneous HR of Uncoated Parts

deg_smooth1=deg_c(1:length(deg_c)-6); %CAD index dropping the last six
values...
                                      %for averaging purposes

%Smoothing the pressure trace
for j=1:length(press_c)-6
    press_smooth1c(j)=(press_c(j+6)+press_c(j+5)+press_c(j+4)...
        +press_c(j+3)+press_c(j+2)...
        +press_c(j+1)+press_c(j))/7;
end

press_coated=press_smooth1c;

deg_smooth2=deg_uc(1:length(deg_uc)-6);


for j=1:length(press_uc)-6
    press_smooth2c(j)=(press_uc(j+6)+press_uc(j+5)+press_uc(j+4)...
        +press_uc(j+3)+press_uc(j+2)...
        +press_uc(j+1)+press_uc(j))/7;
end

press_uncoated=press_smooth2c;

%Plotting the pressure traces and HR traces
plot(deg_smooth1,press_coated,'--',deg_smooth2,press_uncoated,deg_c...
    ,hr_c,'--',deg_uc,hr_uc)
xlabel('Degrees')
ylabel('Pressure (bar)/Heat Release (J/deg)')
legend('Press. Coated','Press. Uncoated','HR Coated','HR Uncoated',...
    'Location','NorthEast')
axis([345 400 -5 75]) %Setting the axis limits
```

B.4 Ricardo WAVE Output Contour Graphing Code

The Ricardo WAVE simulation program was originally developed to model compressible flow through an engine's air intake. Since its conception, the WAVE program has been expanded to optimize all parameters of engine performance. In this study, the WAVE program was used to simulate the effect that compression ratio and heat transfer characteristics has on the fuel consumption of the Yanmar engine. The model did have its limitations due to the fact that every aspect of engine performance, most problematically the combustion duration and phasing, remained constant while the compression ratio and heat transfer characteristics were varied. Because of these limitations, the benefits of reducing the compression ratio were not seen in reality due to the difference in combustion characteristics. It is beyond the scope of this report to go into the details of how the Ricardo WAVE code operates; however, the output from this code from which Figure 3 was created is shown below.

```
clear all
close all

x = [12 12 12 12 12 12;
    13 13 13 13 13 13;
    14 14 14 14 14 14;
    15 15 15 15 15 15;
    16 16 16 16 16 16;
    17 17 17 17 17 17;
    18 18 18 18 18 18;
    19 19 19 19 19 19;
    20 20 20 20 20 20;
    21 21 21 21 21 21;
    22 22 22 22 22 22]

y = [.23 .231 .244 .282 .371 .621;
    .226 .227 .240 .28 .377 .668;
    .223 .223 .237 .279 .384 .727;
    .22 .221 .235 .279 .394 .8;
    .217 .218 .233 .280 .405 .894;
    .215 .216 .231 .281 .418 1.017;
    .214 .215 .23 .283 .433 1.179;
    .213 .214 .23 .286 .449 1.413;
    .212 .213 .23 .289 .468 1.768;
    .211 .212 .23 .292 .49 2.37;
    .21 .211 .23 .296 .514 5.521].*1000

z = [.01 .1 .5 1 1.5 2;
    .01 .1 .5 1 1.5 2;
    .01 .1 .5 1 1.5 2;
    .01 .1 .5 1 1.5 2;
    .01 .1 .5 1 1.5 2;
    .01 .1 .5 1 1.5 2;
    .01 .1 .5 1 1.5 2;
    .01 .1 .5 1 1.5 2;
    .01 .1 .5 1 1.5 2;
    .01 .1 .5 1 1.5 2]



figure
    v = [0:.25:2];
    n=6;
    [C,h]=contour(x, y, z, v,'-k');                % plot contour
    [text_handles]=clabel(C,h, 'LabelSpacing', 300);
    set(text_handles, 'fontsize', 14);
    set(gca, 'LineWidth', 2);
    set(gca, 'FontSize', 16);
    xlabel('compression ratio');
    ylabel('bsfc(g/kW-hr)');
    axis([12 22 200 500]);    %axis([xmin xmax ymin ymax]);
```

B.5 Plot Fixer

```
%Plot Fixer
%Written by: Matt Svrcek  12/05/2001

%Run this script after generating the raw plots.  It will find
%all open figures and adjust line sizes and text properties.

%Change the following values to suit your preferences.  The variable
%names and comments that follow explain what each does and their options.

plotlsize = 2; %thickness of plotted lines, in points
axislsize = 2; %thickness of tick marks and borders, in points
markersize = 8;  %size of line markers, default is 6

%font names below must exactly match your system's font names
%check the list in the figure pull down menu under Tools->Text Properties
%note, the script editor does not have all the fonts, so use the figure menu

axisfont = 'Helvetica'; %changes appearance of axis numbers
axisfontsize = 14;            %in points
axisfontweight = 'normal';    %options are 'light' 'normal' 'demi' 'bold'
axisfontitalics = 'normal';   %options are 'normal' 'italic' 'oblique'

legendfont = 'Helvetica'; %changes text in the legend
legendfontsize = 12;
legendfontweight = 'normal';
legendfontitalics = 'normal';

labelfont = 'Helvetica';  %changes x, y, and z axis labels
labelfontsize = 14;
labelfontweight = 'normal';
labelfontitalics = 'normal';

titlefont = 'Helvetica';  %changes title
titlefontsize = 14;
titlefontweight = 'normal';
titlefontitalics = 'normal';


%stop changing things below this line
%-----------------------------------------------------
axesh = findobj('Type', 'axes');
lineh = findobj(axesh, 'Type', 'line');
axestexth = findobj(axesh, 'Type', 'text');

set(lineh, 'LineWidth', plotlsize)
set(lineh, 'MarkerSize', markersize)
set(axesh, 'LineWidth', axislsize)
set(axesh, 'FontName', axisfont)
set(axesh, 'FontSize', axisfontsize)
set(axesh, 'FontWeight', axisfontweight)
set(axesh, 'FontAngle', axisfontitalics)
set(axestexth, 'FontName', legendfont)
```

```
set(axestexth, 'FontSize', legendfontsize)
set(axestexth, 'FontWeight', legendfontweight)
set(axestexth, 'FontAngle', legendfontitalics)
for(i = 1:1:size(axesh))
   legend(axesh(i))
   set(get(gca,'XLabel'), 'FontName', labelfont)
   set(get(gca,'XLabel'), 'FontSize', labelfontsize)
   set(get(gca,'XLabel'), 'FontWeight', labelfontweight)
   set(get(gca,'XLabel'), 'FontAngle', labelfontitalics)
   set(get(gca,'YLabel'), 'FontName', labelfont)
   set(get(gca,'YLabel'), 'FontSize', labelfontsize)
   set(get(gca,'YLabel'), 'FontWeight', labelfontweight)
   set(get(gca,'YLabel'), 'FontAngle', labelfontitalics)
   set(get(gca,'ZLabel'), 'FontName', labelfont)
   set(get(gca,'ZLabel'), 'FontSize', labelfontsize)
   set(get(gca,'ZLabel'), 'FontWeight', labelfontweight)
   set(get(gca,'ZLabel'), 'FontAngle', labelfontitalics)
   set(get(gca,'Title'), 'FontName', titlefont)
   set(get(gca,'Title'), 'FontSize', titlefontsize)
   set(get(gca,'Title'), 'FontWeight', titlefontweight)
   set(get(gca,'Title'), 'FontAngle', titlefontitalics)
   set(gca, 'Box', 'On');

end
```

Appendix C: Photographic Documentation

Figure 20: Yanmar L48V

Figure 21: Yanmar Piston (Stock)

Figure 22: Yanmar Head and Valves (Stock)

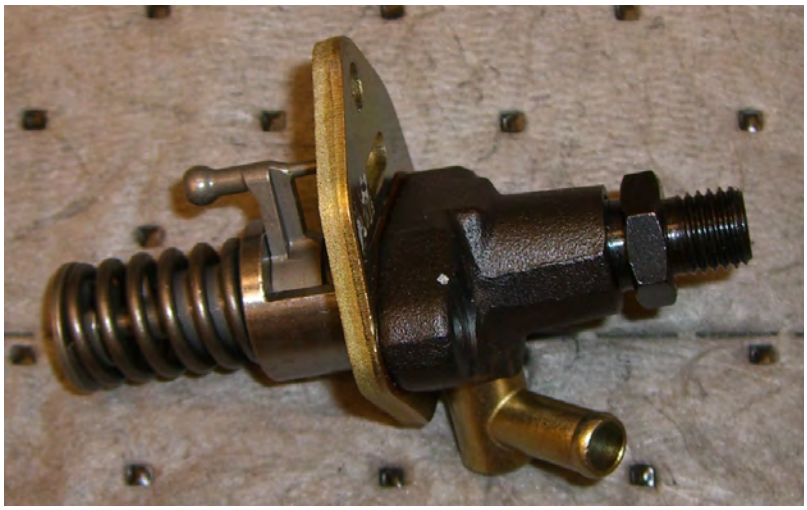

Figure 23: Stock Fuel Pump

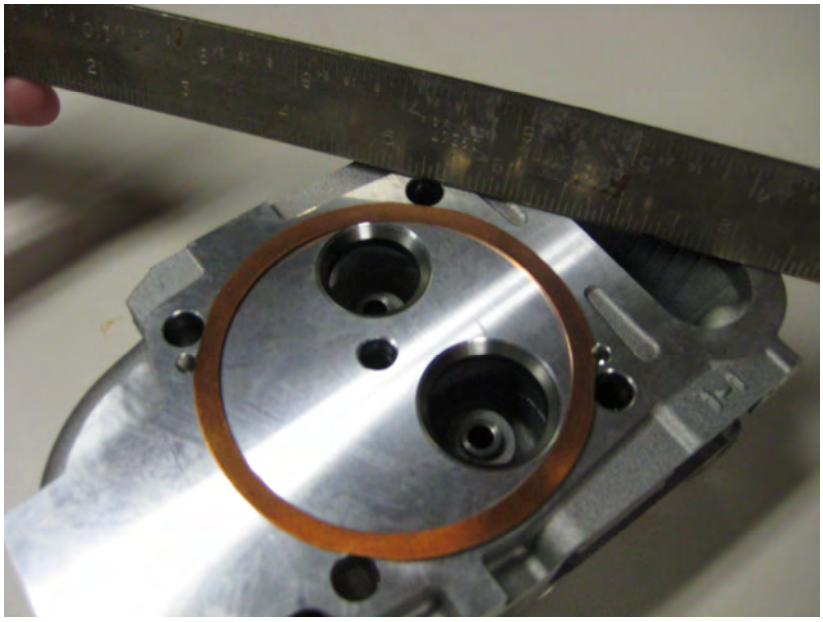

Figure 24: Head with Copper Head Gasket

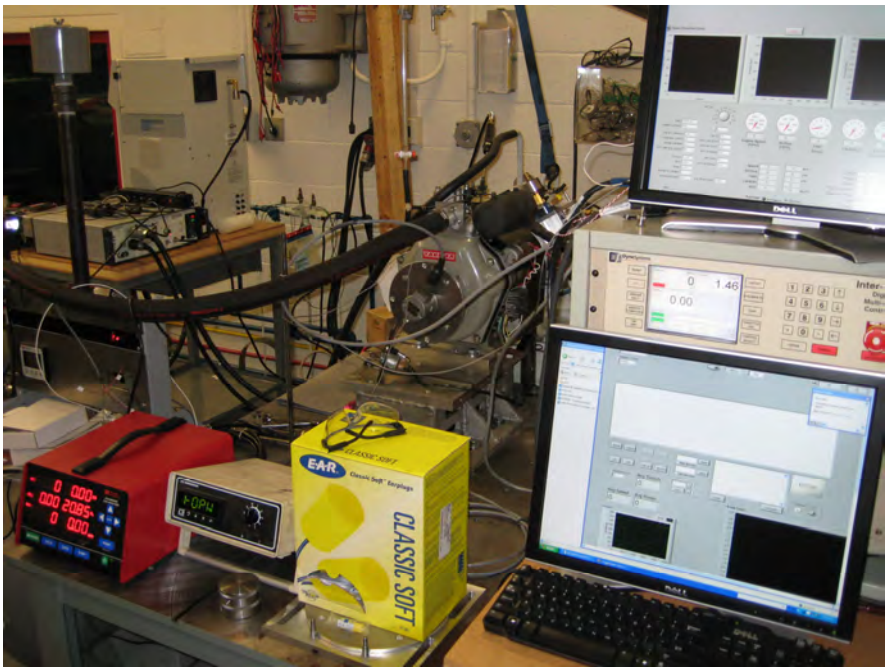

Figure 25: Experimental Setup

Figure 26: Model 66 Midwest and Dynamatic Eddy Current Dynamometer

Figure 27: Dyne Systems Inter-Loc V Digital Multi-Loop Controller

Figure 28: Omega Thermocouple

Figure 29: Omega Monogram Ten-Channel Thermocouple Reader

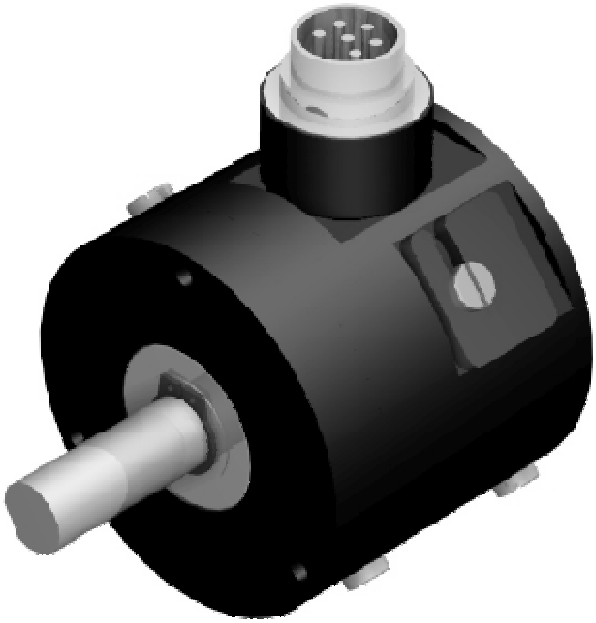

Figure 30: Digital Shaft Encoder

Figure 31: Infrared and Chemical 5-gas Analyzer (IM Type InfraRed Industries)

Figure 32: Piezo-electric Pressure Transducers (Kistler 6052C and Kistler 4067)

Figure 33: Kistler Amplifier Type 5010

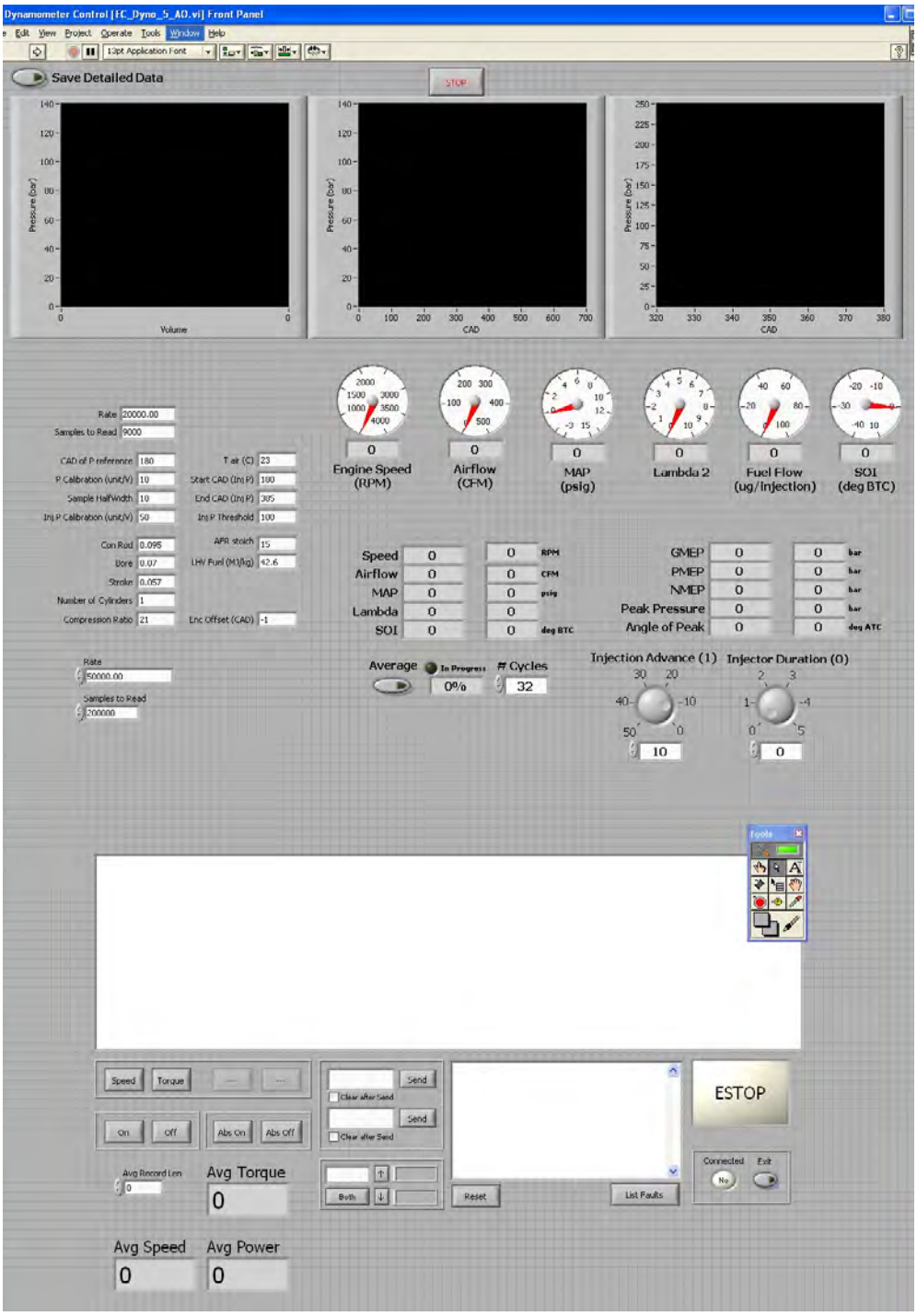

Figure 34: LabVIEW User Interface

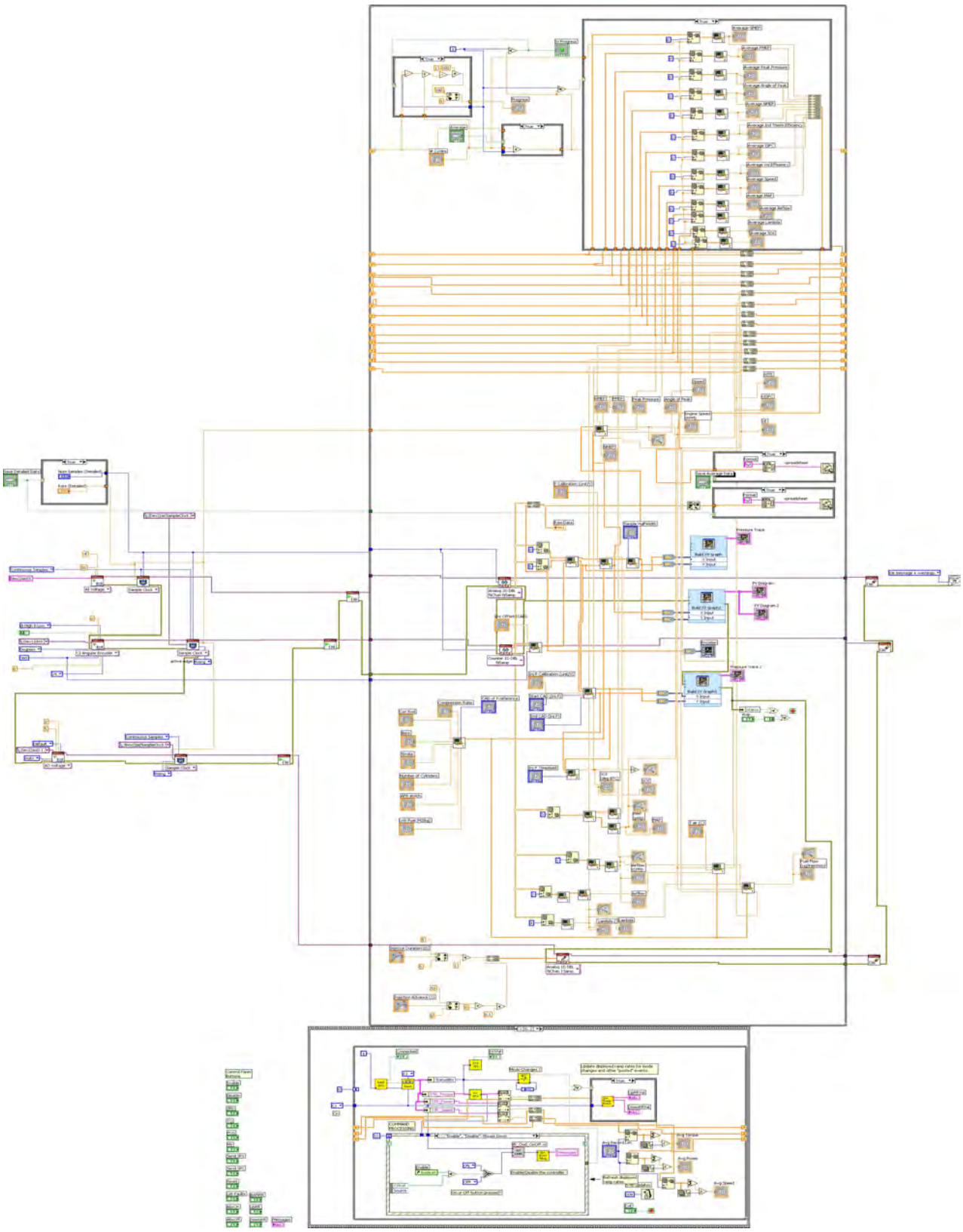

Figure 35: LabVIEW Block Diagram

Figure 36: Air Flow Damper Tank System

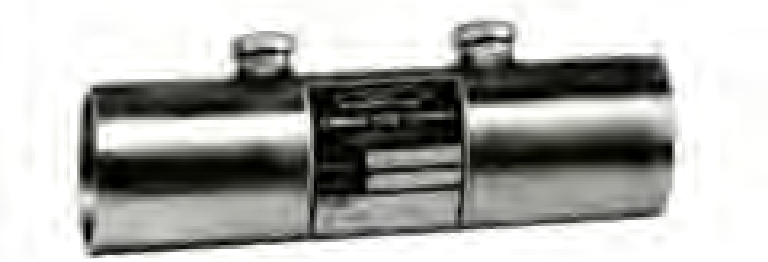

Figure 37: Meriam Instruments Laminar Flow Element

Figure 38: Meriam Instruments 2100 Series Smartgauge

Figure 39: Digital Scale 10 lb Capacity

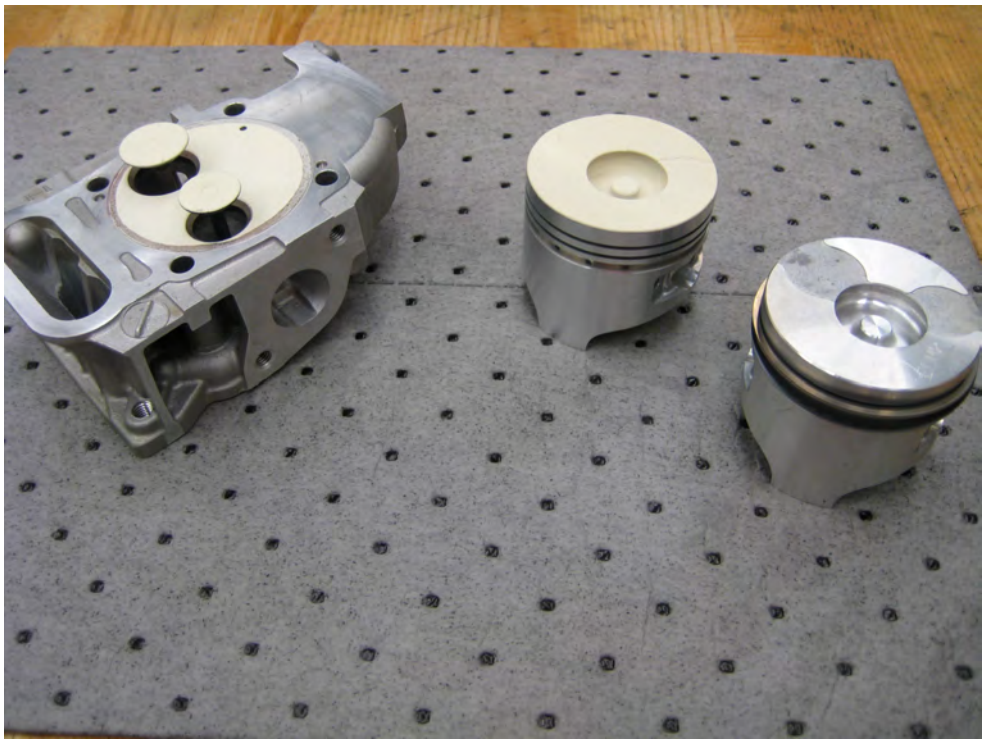

Figure 40: Head, Valves, and Piston with TBC Compared to Uncoated Piston

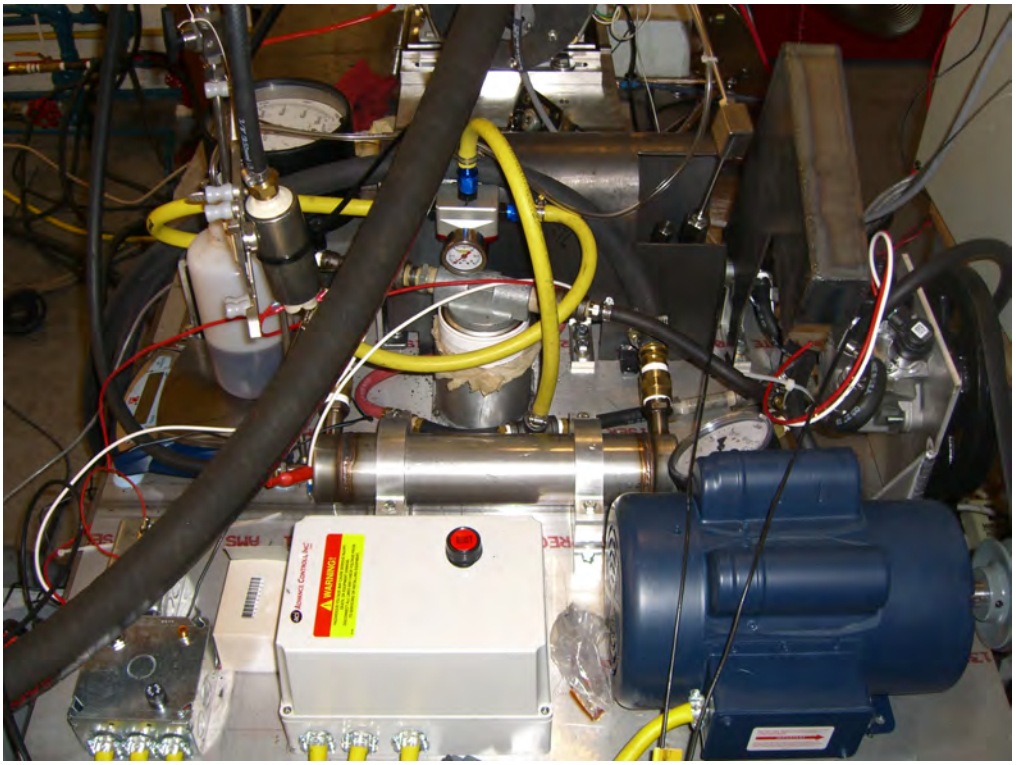

Figure 41: HP Fuel Injection Platform

Figure 42: 80/20 Aluminum Strut

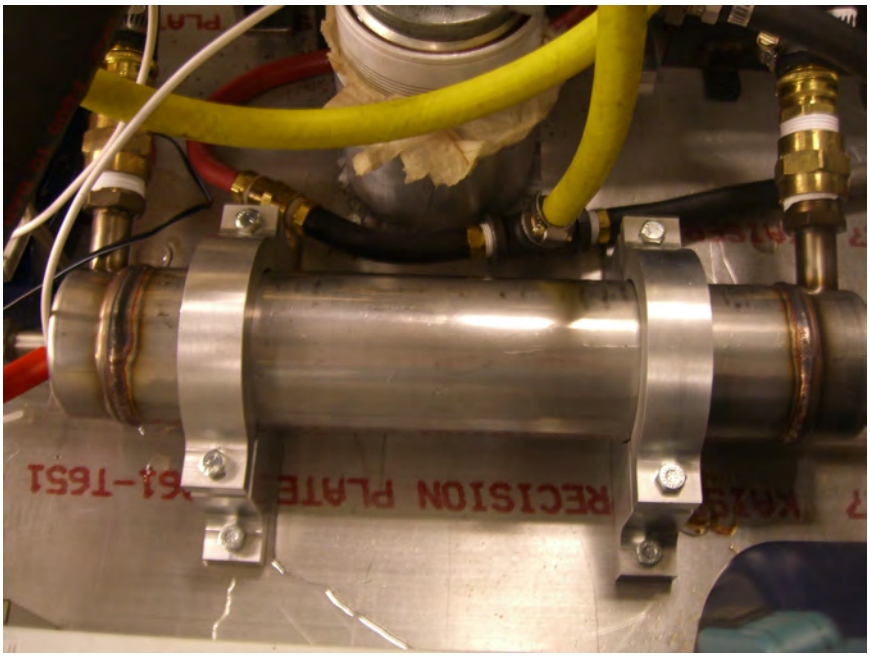

Figure 43: Heat Exchanger

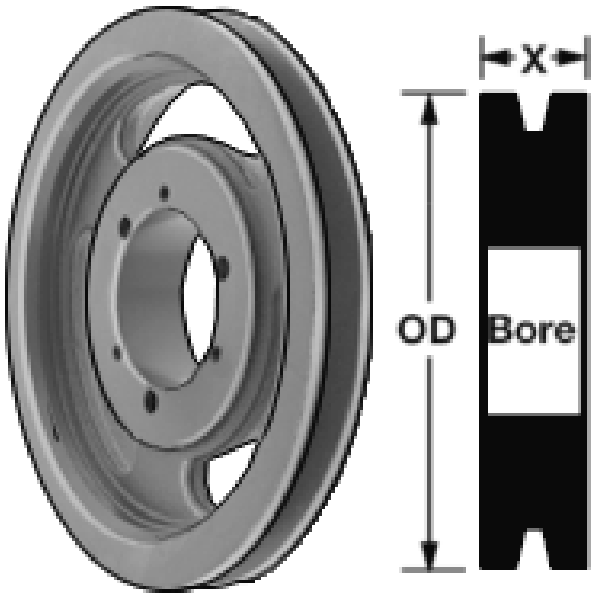

Figure 44: 8.95" OD Quick-Connect Pulley on HP Fuel Pump

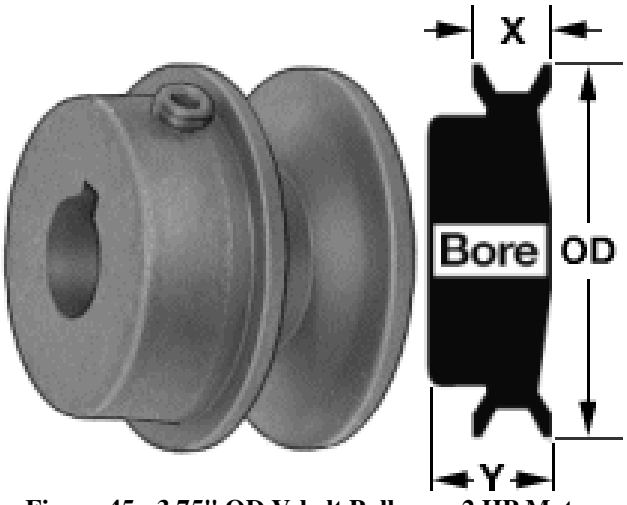

Figure 45: 3.75" OD V-belt Pulley on 2 HP Motor

Figure 46: 60,000 psi Fuel Line Cone and Threading

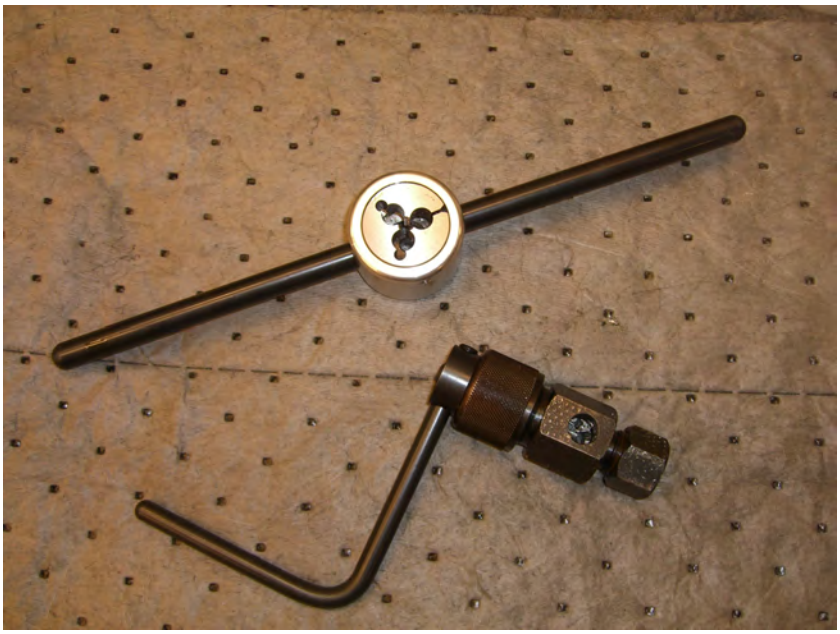

Figure 47: Coning and Threading Tools for HP Tubing

Figure 48: HP Union

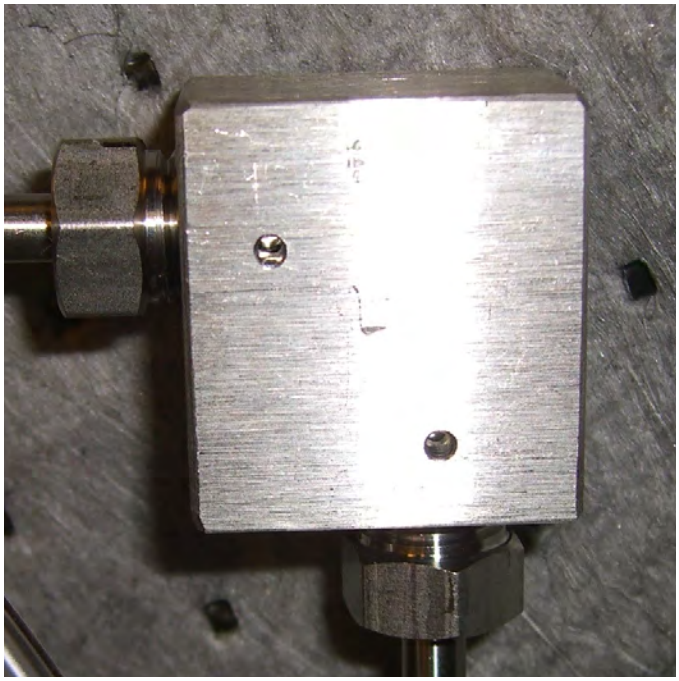

Figure 49: HP Fuel Line Elbow

Figure 50: HP Burst Caps

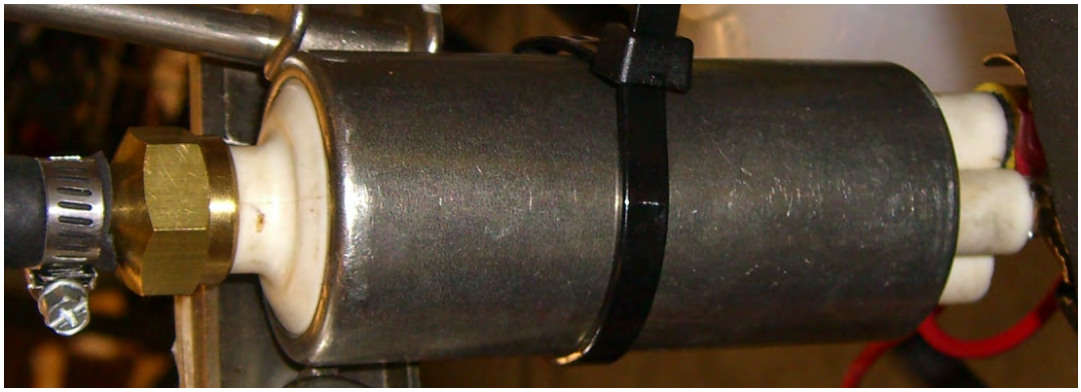

Figure 51: 50 psi Inline Fuel Pump

Figure 52: Leeson 1725 rpm 2 HP Electric Motor

Figure 53: Enclosed Non-Reversing Motor Starter W/ Overload Relay, 22 to 30 Amp Overload

Figure 54: Fuel Filter

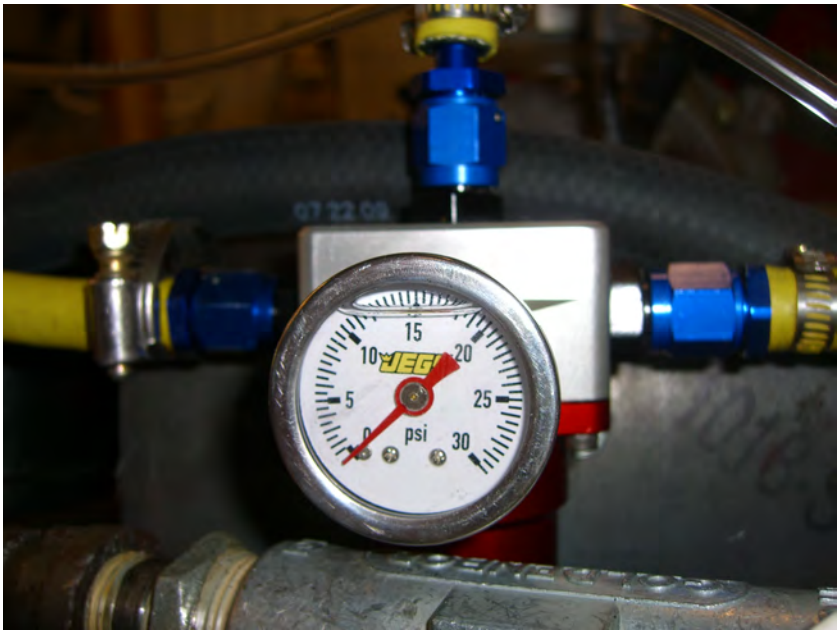

Figure 55: LP Fuel Pressure Regulator

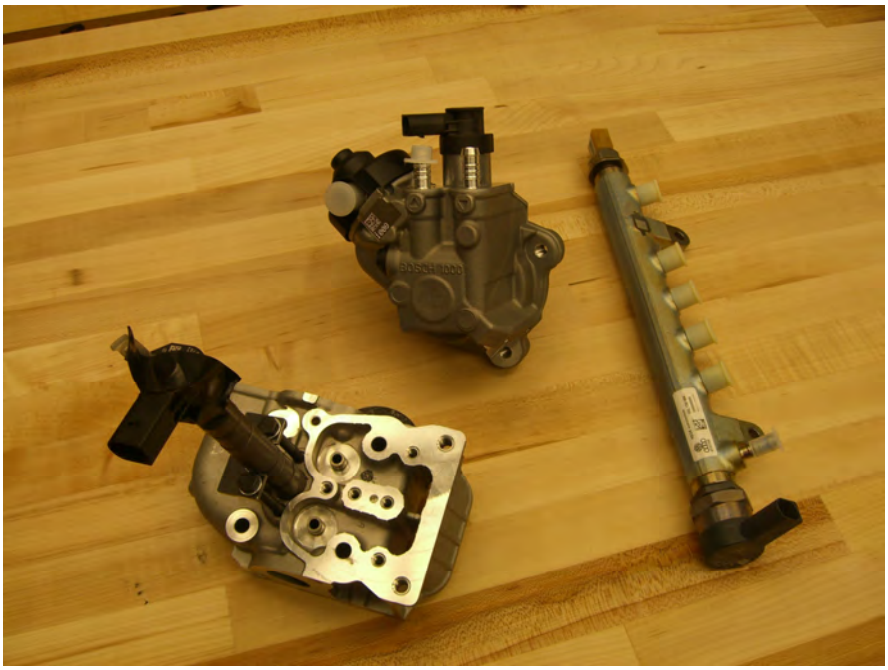

Figure 56: Bosch Common-Rail, CP 4.1 HP Pump, and Injector in Head

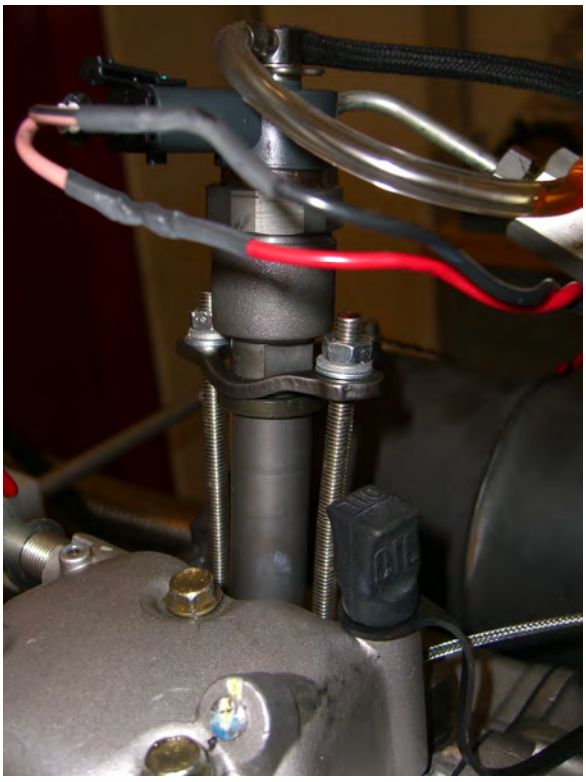

Figure 57: Bosch Solenoid Injector

Figure 58: High Pressure Equipment Model 6PG50 Fuel Pressure Gauge

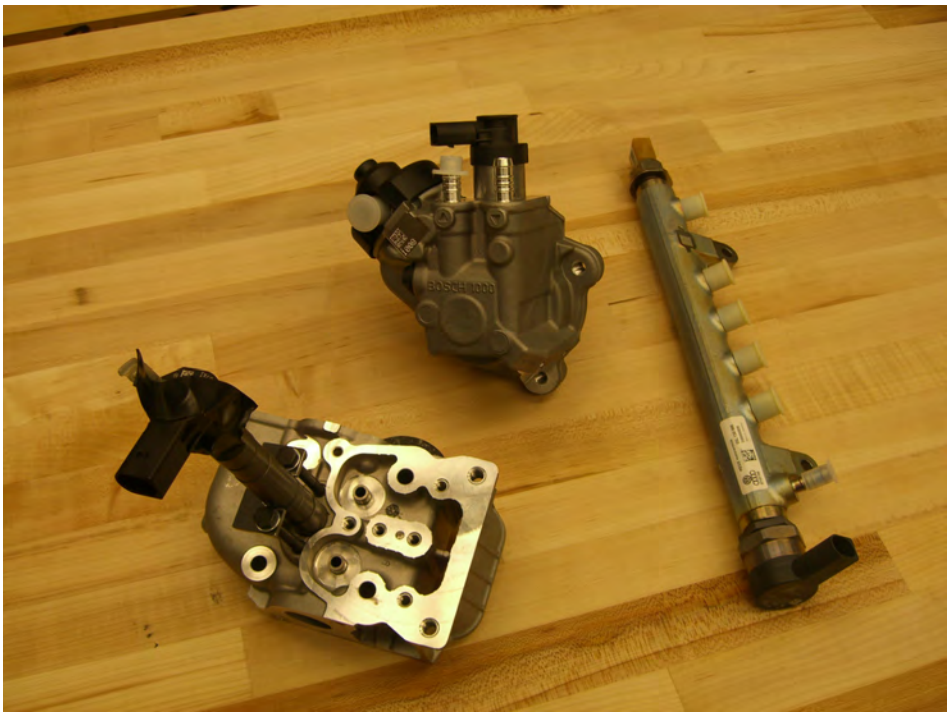

Figure 59: Bosch CP 4.1 HP Pump, Common-Rail, and Injector

Appendix D: Detailed Instrumentation Information

This section outlines the instrumentation fitted to the Yanmar L48V Diesel engine. The engine was highly instrumented in order to facilitate a first law energy flow analysis. Some of the instrumentation also allowed for exhaust gas analysis which provides valuable emissions data that can be used to analyze the combustion efficiency.

The instrumentation included piezoelectric pressure transducers in the fuel line for SOI analysis, and the combustion chamber for engine cycle analysis. Gas sample ports and a thermocouple were placed in the exhaust manifold for exhaust enthalpy and chemical analysis. The crankshaft was also coupled with a dynamometer to measure the engine's torque and speed. An encoder was also placed on the crank shaft to measure its angular position. An air flow analyzer was connected to the engine's intake manifold. The shaft encoder, pressure transducers, and dynamometer feed all data into a data acquisition program called LabVIEW. The following sections discuss each item in detail, giving background on how the instrument works and how the measurement is important to the study.

D.1 Piezoelectric Pressure Transducers

Piezo-electric pressure transducers were placed in the head (Kistler 6052C) and the fuel line (Kistler 4067) to gain data on in-cylinder pressure and start of injection data respectively. These pressure sensors take advantage of the piezoelectric effect in which certain crystals produce an electrical output when subjected to changes in mechanical loading. Crystal sensors are the standard for engine research today due to their robust mechanical properties, high sampling rate, and broad-spectrum accuracy.

The crystals produce a charge on the order of pico-Coulombs and therefore need to be passed through a high impedance amplifier (Kistler Amplifier Type 5010) that converts the charge into a measureable voltage. In this study the voltage data were collected using a high speed data acquisition system called "LabVIEW". The data stream is synchronized with the crank angle degree (CAD) indicator, an electronic device connected to the crank shaft which sends a signal every degree. While the maximum data rate for the piezoelectric sensor is 100 kHz, this study only utilizes a rate of 50 kHz. This lower data rate provided fine enough resolution while not overtaxing the data acquisition system.

D.2 Exhaust Gas Analyzer

Exhaust gas composition data were collected using an infrared and chemical 5-gas analyzer (IM Type InfraRed Industries). This machine measured quantities of carbon dioxide, hydrocarbons, nox, carbon monoxide, oxygen, and the air fuel ratio. This data can be used to analyze the performance of the engine, and was also used to run a real time diagnostic on the engine: in that

as the operating conditions were modified, the unburned hydrocarbon count was monitored to determine if excessive amounts of soot were being produced. If the soot production exceeded a certain threshold the tests would be terminated. Once high soot levels were present, it becomes clear that the engine is not operating efficiently and any further time spent gathering data would be wasted. The Yanmar presented a difficult situation with the gas analyzer due to high levels of soot formation in the engine during high load levels. These high soot levels clogged the filters and required frequent downtime to flush the filters to maintain accurate readings.

D.3 Dynamometer

There are two pieces of information necessary to calculate the efficiency of the engine. First, the amount of fuel that is consumed during a specific amount of time must be determined. This can be done one of two ways. The first technique used in this study is to fill a graduated cylinder with fuel, then start a stop watch while the engine is running and record the amount of time it takes to consume a specific volume of fuel. A second technique that was used once the common-rail was implemented was to have a fuel tank rest on a scale, then record the initial and final mass of the tank over a period of time. Both methods are highly accurate, the first utilizing volume and the second utilizing mass.

Once the fuel consumption was determined, the corresponding power output during this timeframe must also be measured. This can be accomplished by coupling the engine to a dynamometer. A Model 66 Midwest and Dynamatic Eddy Current Dynamometer was used to gather this data. The Eddy Current Dynamometer was controlled by a Dyne Systems Inter-Loc V Digital Multi-loop Controller and it allowed the user to control multiple variables of engine performance, i.e. engine speed or torque levels. In this case, the engine speed was set at 2750 rpm. The dynamometer was interfaced with LabVIEW and produced instantaneous readouts for engine speed, torque, and horsepower. LabVIEW was also used to produce an average value for horsepower and torque based on a user defined number of samples. In this case the number of samples for an average was set at 100 cycles.

D.3.1 Calibration

The dynamometer was calibrated using the user interface panel on the Dyne Systems controller. While the engine is not in operation, the user first zeros the system by pressing calibrate, then zero. The dynamometer readout slowly returns to zero. Once a zero reading is obtained, the user presses “Save”, then places a twenty pound weight on an eighteen inch arm that extends straight out from the body of the dynamometer. The user then must press “Span” and enter a torque of thirty ft-lbs. Once the readout settles on this number, the user presses “Save” and the dynamometer has been successfully calibrated.

D.4 Air Flow Analyzer

In order to run diagnostics on the combustion process in regards to volumetric efficiency and exhaust gas production, the amount of air that is flowing into the cylinder must be measured. One of the major problems with analyzing the air flow of a four-cycle engine during operation is the pressure fluctuations in the intake manifold. Due to the fact that the engine is only drawing

in air for a quarter of the time that it is operating, the instantaneous air flow reading would fluctuate wildly if an instrument was place directly on the intake manifold. In order to average out the air flow and provide a more reliable reading, a damping system was constructed.

The damper system that was constructed by MIDN Doug DeVuono is being utilized in this study. The system consists of a twenty gallon damper tank, a Meriam Instruments Laminar Flow element, and a Meriam Instruments 2100 Series Smart gauge. The air is drawn into the tank and passes through the Meriam laminar flow element. Tubing is connected to either end of the element and is fed directly into the smart gauge. This gauge measures the pressure drop in the air and automatically calculates the volumetric air flow rate in ft^3/min by taking into account the known geometry and fluid properties of the laminar flow element, then displays this information on a digital readout.

D.5 Exhaust Thermocouples

The enthalpy of the exhaust gases is a critical piece of information to quantify the amount of energy being lost as wasted heat through the exhaust pipe. A simple way to calculate the enthalpy of these gases is to measure their temperature using a thermocouple placed close to the exhaust port, inside the exhaust pipe. One of the byproducts of insulating the combustion chamber with thermal barrier coatings is that the exhaust enthalpy should rise. While this study makes no attempt to harness this increase in energy of the exhaust gases, the increase was measured for comparison to the stock values.

Thermocouples are constructed by welding two wires together that consist of differing alloys. The coupling of these alloys produces a voltage that is in proportion to the temperature. When choosing a set of alloys for a thermocouple it is important that these metals produce predictable and repeatable voltages across the range of temperatures in which the instrument will be used. In this study the thermocouple voltage was converted to a temperature reading by a converter. A Monogram ten-channel thermocouple reader manufactured by Omega was used to obtain the temperature readings from the exhaust manifold.

D.6 LabVIEW

In order to gather and process the large amount of data streaming from the pressure transducers and the dynamometer, a computer program known as “LabVIEW”, short for Laboratory Virtual Instrumentation Engineering Workbench, was programmed for operation during this study. This program allowed for the easy operation of speed settings on the dynamometer and allowed for a set number of measurements to be averaged from the dynamometer in order to provide more stable torque and power readings. LabVIEW also had displays of real-time pressure versus volume graphs and pressure versus crank angle degree. Internal computations in the program output the **gross mean effective pressure** (GMEP), **friction mean effective pressure** (FMEP), **net mean effective pressure** (NMEP), peak pressure in bar, and angle after **top dead center** of the peak pressure. One of the most useful features of LabVIEW was its detailed data gathering ability. Upon command the program would record the pressure transducer voltages at a rate

specified by the user for a time period of six seconds. This study used a data collection rate of 50 kHz. The large data file could then be extracted for detailed data analysis using MATLAB.

Appendix E: Engine Modification

This section outlines the modifications made to the test engine for the purposes of increasing its efficiency. The engine's performance was first tested by varying the compression ratio incrementally. Next the engine was converted to a LHR engine with the application of thermal barrier coatings and the compression ratio sweep was repeated. Finally a common-rail fuel injection system was mated to the engine while maintaining the LHR characteristics and the compression ratio was set to the stock value of 21. With the application of both the thermal barrier coatings and the common-rail system the SOI was adjusted at each compression ratio to achieve maximum efficiency.

E.1 Compression Ratio

There were two candidate concepts initially considered to reduce the compression ratio of the Yanmar engine. The first concept involved enlarging the bowl on the face of the piston for each compression ratio. The bowl is a small cup on the top of the piston that is commonly used in production Diesel engines today. The bowl acts as the initial combustion chamber and is the location the fuel is injected. Great care is taken in the geometric design of the bowl as its shape affects the swirl of the fuel as it enters the chamber and can have an affect on combustion efficiency. Enlarging the bowl had the benefit of maintaining the same **squish height** throughout the testing, which would in turn minimize the colder surfaces in the engine that are exposed to fuel. The major problems associated with this approach are that the carefully planned geometry of the bowl would be modified and therefore the effects this modification has on engine performance are unpredictable. Also when thermal barrier coatings were applied to the piston face, it would have been necessary to have three pistons custom coated for this study instead of just one. Finally the structural integrity of the piston face potentially could have been compromised. At the bottom of the bowl, the piston is very thin and a further reduction in its thickness could have potentially produced a catastrophic piston failure in which the bottom exploded outward due to the overwhelming pressures present during the combustion process.

The more feasible approach was to increase the squish height by adding head gaskets of appropriate thicknesses for each compression ratio. The compression ratio was incrementally reduced using copper head gaskets adding an additional 0.505 mm of clearance for a compression ratio of 18:1 and 0.953 mm from stock for a compression ratio of 16:1. Adjustments to the valve clearance settings were necessary to maintain proper valve opening while high temperature sealant was applied to the push rod chamber to maintain oil-tight integrity. One of the negative aspects of this approach is that the overall heat transfer characteristics of the combustion chamber are increased, which means that more heat produced during the combustion process escapes through the cylinder wall due to both the increased surface area, but also the increased thermal conductivity of the copper versus the aluminum out of which the engine is originally constructed. This process also changes the relative position of the fuel injector in relation to the bowl. The geometric design of the bowl may not be fully utilized and the combustion efficiency may be slightly reduced. The benefit of using this technique is that it requires no special machining techniques, and is therefore much more cost

and time effective. This technique also eliminates the need to coat multiple pistons with the thermal barrier coatings.

E.2 Thermal Barrier Coating

Thermal barrier coatings consist of a ceramic material that has high **thermal impedance**. These coatings are placed on the face of the piston, the valve faces exposed to the cylinder, and the surface of the head that is exposed to the cylinder. The purpose of these coatings is to insulate the combustion chamber and force more of the heat of combustion into work instead of simply escaping through the engine block as waste heat. Ceramic materials are commonly used to insulate engines and have generally shown improvement in engine efficiency. Problems with thermal coatings are that they have very poor fatigue strength, often failing in brittle fracture mode. Therefore it is currently not possible to construct engines completely consisting of ceramics. It is also difficult to apply ceramics to the cylinder walls because of the high level of fatigue loading this area experiences.

Taking into account the material properties of these thermal coatings, it was determined that only the pressure loaded surfaces would be coated. The pressure loaded surfaces are those listed at the beginning of this section. This study conducted testing on two thicknesses of thermal barrier coatings. Initially a 0.004" thick polymer ceramic was used to test the performance of the engine. This coating performed poorly, adding little, if any improvement to fuel consumption and therefore a thicker 0.015" thick yttrium stabilized zirconium ceramic was placed in the engine. Coating the piston face, valve faces, and head was outsourced.

E.3 Mechanical Fuel Pump Adjustments

Optimal fuel injection timing is phased such that the maximum spike in pressure occurs when the crank shaft is approximately seven to eight degrees after top dead center (TDC). The purpose of optimizing fuel injection timing is to maximize the work produced by each combustion cycle. It is in this region of seven to eight degrees after TDC that there is a balance between maximum pressure and maximum change in volume, which results in a maximization of work production. Since the conditions inside the combustion chamber were changed with each engine modification, i.e. compression ratio adjustment and the addition of the thermal barrier coatings, it was necessary to adjust the SOI to achieve the peak pressure rise in that optimal region.

The first battery of testing was completed using the stock mechanical pump. This pump was adjustable by the use of shims that were placed beneath the pump and delayed or advanced the SOI when added or removed respectively. The shims allowed for a delta in SOI of 0.25 crank angle degrees by the addition of a 0.001" thick shim. The mounting plate for the pump was also machined thinner to allow for a greater advancement in SOI than allowed by the original design. All references in the results section that refer to degrees of SOI advance are referring to the stock pump with the stock mounting plate.

E.4 Common-Rail Injection System

In order to test the effects of high pressure fuel injection, a common-rail fuel injection system was adapted for use on the Yanmar engine. The parts for this system were originally designed for use in the Volkswagen Jetta 2.0L TDI engine and can be seen in Figure 59. This system was chosen for its small capacity and variable pressure capabilities. A photo-journal detailing all the parts used for construction of this apparatus can be seen in Figures 39 and 41-59.

A schematic of the fuel system design is shown in Figure 60. The fuel is first drawn from the fuel tank by a 3.5 bar lift pump and is passed through a pressure regulator to achieve an inlet pressure at the Bosch CP 4.1 high pressure pump of 1.5 bar. This feed pressure is necessary to overcome a check valve located at the inlet to the high pressure pump. The fuel is also passed through a filter before entering the high pressure pump to remove any contaminants from the lab environment.

The Bosch pump boosts the fuel pressure from 1.5 bar to a user defined pressure ranging from 340-2000 bar. A simple 12 volt, square wave, 300-1000 Hz signal was fed to the pressure regulating valve on the rail. By adjusting the duty cycle and frequency, the desired rail pressure could be achieved. The pressure gauge shown in Figure 58 is connected to the accumulator rail and is used to monitor the performance of the pump and serves as an easy way to ensure the pressure of the system does not exceed its design limits. If this should occur, an emergency burst cap is in place on the high pressure side that will dump the fuel into an auxiliary tank. A separate line also is taken from the accumulator and is sent to the fuel injector for consumption in the engine. The electronic control of the injector will be discussed later.

The excess fuel is returned back to the fuel tank after passing through a heat exchanger. Also connected to this return line is the return from the pressure regulator on the feed line, and a relief line stemming from a valve on the pump that was not utilized during this study. Due to the much smaller gross fuel consumption of the Yanmar as compared to the Jetta, a high percentage of the fuel is circulated through the system before it is consumed. The fuel is heated every time it passes through the Bosch pump; therefore it was necessary to include a heat exchanger in the system to avoid excessive heat build up in the fuel.

The purple block shown just below the fuel tank is a shutoff valve that allows the user to isolate the fuel system once it is primed to eliminate the need to prime the system before each use. Not shown in Figure 60 is the scale on which the fuel tank rests. This scale was used to record the mass of fuel consumed over a given time for fuel consumption data.

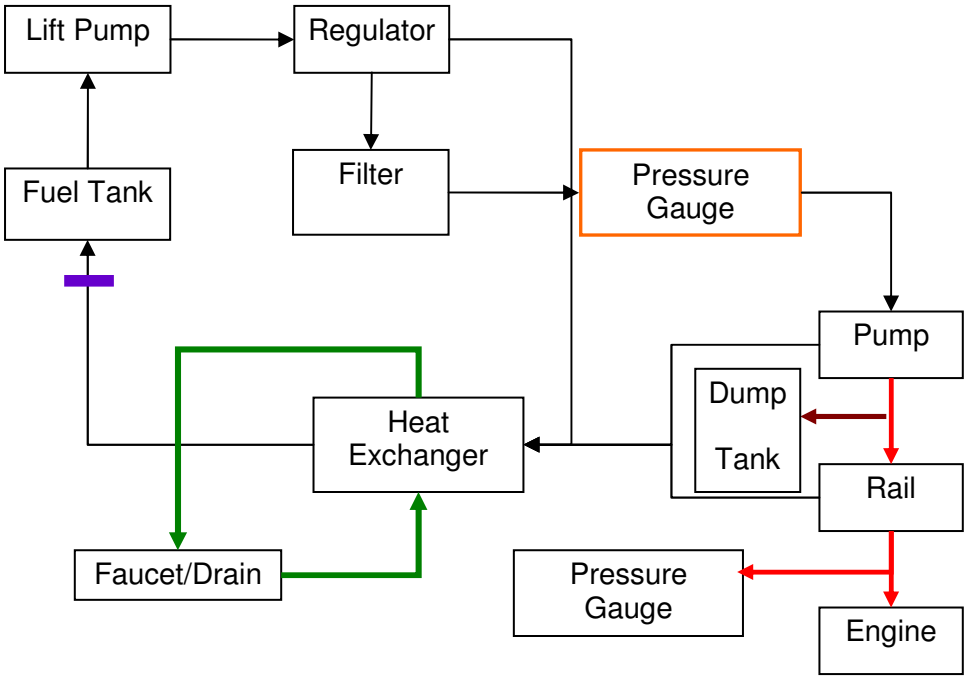

Figure 60: Schematic of the Common-Rail System

There are several electrical sub-systems on this fuel platform. The first of which is the power circuit for the electric motor as shown in Figure 60. During startup, the 2 HP electric motor requires high amperage. In order to handle the large current, a motor controller was wired into the system. This controller consists of a magnetic switch that is capable of passing large amounts of current without overheating or burning out the switching mechanism. It is operated by energizing the magnetic switch which snaps together and allows electricity to flow to the motor for operation. The magnetic switch is represented in Figure 61 by the brown box inside the motor controller. Note that the same lines that energize the switch also power the motor. The benefit of this setup is that the switching mechanism only requires a low voltage, thereby reducing the stress placed on the first switch. A light was placed on the wiring that controls the magnetic switch to indicate if power is flowing to the magnetic switch and therefore indicating whether the electric motor should be spinning.

There are two fail-safes in this system. The first one is in the motor controller. A load control circuit senses if the magnetic switch is heating up, or if too high a load is being placed on the switching mechanism for safe operations. If too high a load is placed on the switch, the magnet cuts out and the circuit is broken. The second fail-safe is located on the electric motor. It is cutout circuit similar to the one in the motor control except that it is not load adjustable.

A fuse was placed above the motor controller as an added fail-safe; however, the required size of fuse was not available and therefore it was removed. A major difference between the overload circuit and a fuse is that the overload circuit only cutouts after heat builds up from prolonged

overload. A fuse on the other hand is an instantaneous cutout that fails as soon as the current exceeds the fuse's maximum capacity.

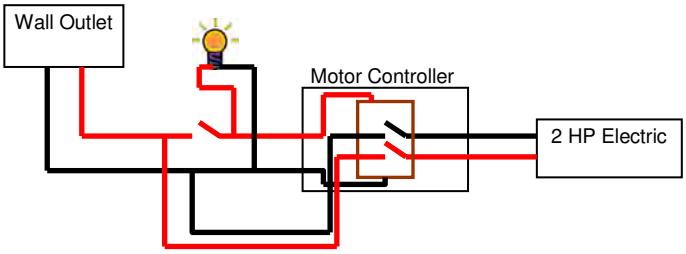

Figure 61: Wiring Schematic for the 2 HP Electric Motor

Another simple circuit was constructed to operate the low-pressure lift pump and is shown in Figure 62. This pump is powered by a 12 VDC car battery in order to simplify the power source requirements. Instead of having to step down and rectify the 120 VAC electricity coming from the wall, the car battery provides a consistent source of electrical power to operate this low-pressure pump.

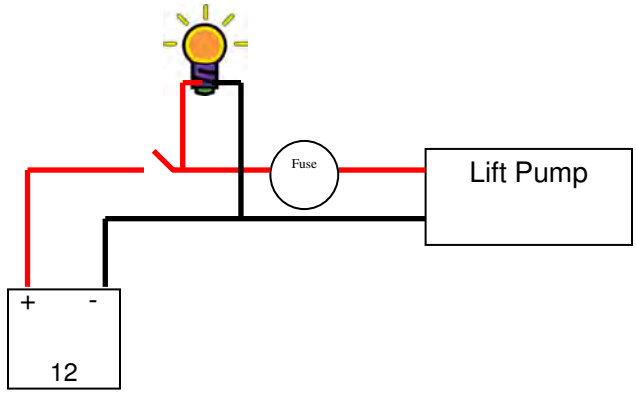

Figure 62: Wiring Schematic for the Lift Pump

E.4.1 Fuel Injector Peak and Hold Circuit and Driver

The fuel injector used in this study was a solenoid powered, computer controlled injector as seen in Figure 57. In order to operate this injector, a circuit was designed and implemented that constructed a peak-and-hold wave form. An ideal representation of this waveform can be seen in Figure 63. Due to the high pressure associated with this injection system, a high current must be initially sent through the injector just to open the valve. In order to prevent burning out the fuel injector with continued high current, once the valve is open it is necessary to drop the current to a holding level that is sufficient to maintain the open position until the desired injection duration was reached.

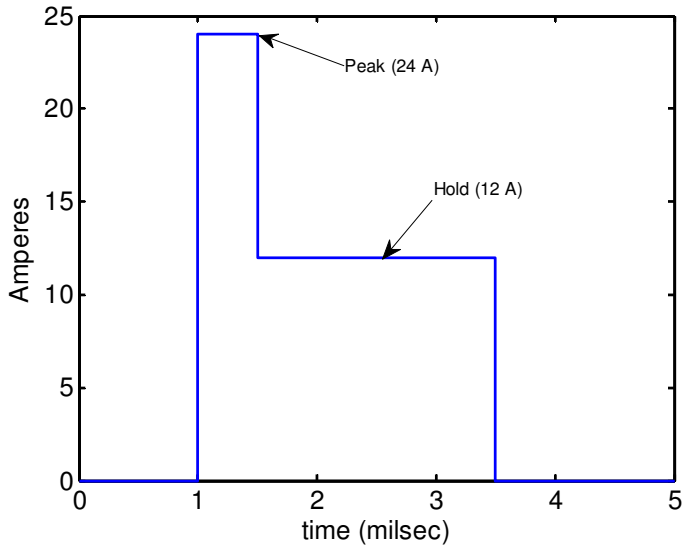

Figure 63: Peak and Hold Waveform

The schematic for the driving circuit can be seen in Figure 64. Because the injector is a large solenoid, it has a large inductance and minimal resistance. Upon receiving signal from the PIC microprocessor, the two MOSFET transistors would close, allowing 25 volts to flow through the injector to ground. After 400 microseconds the peak signal was shut off, which opened the circuit for the 25 volt source. The low side MOSFET remained on causing the voltage to drop until the diode leading to the battery became forward biased, causing the battery to supply the hold current. Once the desired amount of fuel was injected, typically after 1 millisecond, the low side MOSFET was opened by the PIC causing the injector to shut.

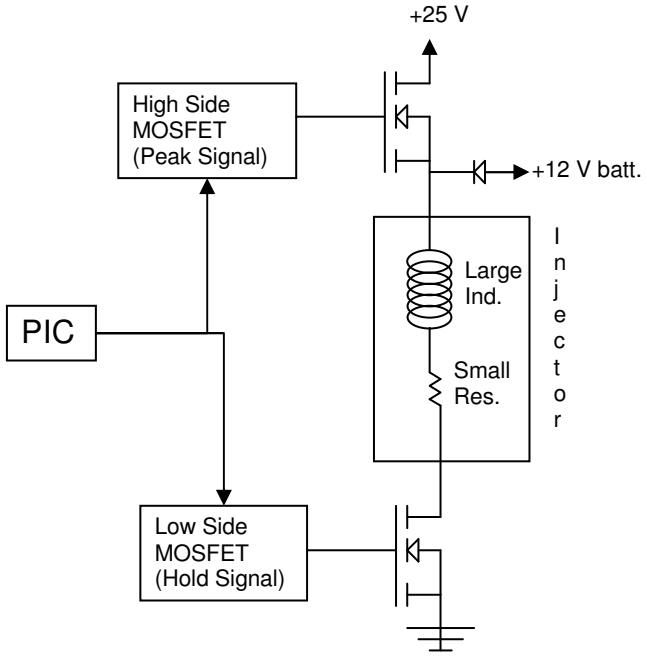

Figure 64: Peak and Hold Circuit

The timing for this waveform circuit was controlled by a PIC (Programmable Interface Controller) microprocessor. It is beyond the scope of this study to explain the inner workings of this microprocessor; however, the code driving this processor is shown in Appendix E.4.1.1. This code compares the crank angle degree data to the pressure transducer data. The shaft encoder sends out a pulse at TDC, then at each CAD. The code looks for when the crankshaft is at TDC with a low pressure. These criteria indicate that the engine is just finishing its exhaust stroke and the next time the piston approaches TDC the injector is instructed to inject fuel to the cylinder. Once the command to inject is given, the PIC closes the MOSFETs initiating the peak and hold wave form.

E.4.1.1 PIC Controller Code

```
#include <18F252.h>
#device ADC=10
#include "C:\Program Files\PICC\Drivers\stdio.h"

#use delay(clock=10000000)
#fuses NOWDT,RC, NOPROTECT, BROWNOUT, NOLVP, HS
#use rs232(baud=9600,parity=N,xmit=PIN_C6,rcv=PIN_C7,bits=8)
long count,adpress,adfuel,fuel,injfinal,adtime;
int injon,portbb,byteb,injadj;
#INT_EXT
void isr_bint0(void)
{
//one pulse per rev encoder index
output_high(pin_c0); //for diagnostics
count=0;
enable_interrupts(INT_EXT1);
}
#INT_EXT1
void isr_bint1(void)
{
//count crank angle degrees
count=count+1;
if (count==330){
output_low(pin_c0);   //end of diagnostic
set_adc_channel(0);    //in-cylinder pressure
delay_us(5);
adpress=read_adc();
}         //end above if
if (count==injfinal && adpress>=50){
//         output_low(pin_c0);
           output_high(pin_c1);  //peak activate
           output_low(pin_c2);
           injon=1;
```

```
        set_timer0(65000);     //1000 ticks w/ 10MHz clock = 400 usec  64535
}       //end if
}       //end interupt 1
#INT_TIMER0
void clock_isr0(void)
{
if(injon==1){
//output_high(pin_c2);          //hold activate
output_low(pin_c1);             //end peak
set_timer1(fuel);
injon=0;
}       //end if
}       //end inttimer0
#INT_TIMER1
void clock_isr1(void)
{
output_high(pin_c2);
}
void main()
{       //start of main
  setup_spi(FALSE);
  setup_timer_0(RTCC_INTERNAL);
  setup_timer_1(T1_INTERNAL | T1_DIV_BY_2);   //same as timer 0 which is default div.by 2
  setup_timer_2(T2_DIV_BY_16, 255, 1);
  setup_timer_3(T3_INTERNAL|T3_DIV_BY_1);
  setup_ccp2(CCP_OFF);
  setup_ccp1(CCP_OFF);
  setup_adc(adc_clock_internal);
  setup_adc_ports(RA0_RA1_RA3_ANALOG);
  set_tris_a(0xff);    //RA0, RA1 and RA3 are analog
  set_tris_b(0xff);      //B outputs   1=in, 0=out
  port_b_pullups(true);
  set_tris_c(0x00);    //PC0 used for LED/Debug,PC1 pwm2, PC2 pwm1, PC6 is TX, PC7 is RX
//setup_port_a( ALL_ANALOG );
        output_low(pin_c3);
        output_high(pin_c2);
        output_low(pin_c1);
        output_low(pin_c0);
   output_low(pin_c4);
        EXT_INT_EDGE(0, L_TO_H);
        EXT_INT_EDGE(1, L_TO_H);
        EXT_INT_EDGE(2, L_TO_H);
  enable_interrupts(INT_EXT);
  enable_interrupts(INT_TIMER0);
  enable_interrupts(INT_TIMER1);
  disable_interrupts(INT_EXT1);
```

```
   enable_interrupts(GLOBAL);
count=0;
injon=0;
set_adc_channel(0);
while(1){
// fuel injection duration (hold)
set_adc_channel(1);
delay_us(10);
adfuel=read_adc();      //ain1=fuelamount
fuel=65535-6*adfuel;
// fuel injection timing
set_adc_channel(3);
delay_us(10);
adtime=read_adc();     //ain2=injection timing
//logic for injection timing adjustment
//portbb=input_b();
//byteb=portbb>>2;
//byteb&=0x0f;
//injadj=injadj*2;
injadj=adtime/20;  //quick approx. check w/ 5v=1024/20 = 50deg
if(injadj<2)injadj=2;
if(injadj>32)injadj=30;
injfinal=359-(long)(injadj);    //integer of injection timing 360=TCC
// end of injection timing adj.
}         //end of while(1)
}         //end of main
```

E.4.2 Users' Manual

1. Ensure the valve above the fuel tank is open to allow fuel to be pulled into the system.
2. Check that there are no obstructions in the belt or pulley that drives the high pressure pump.
3. Check for any obvious damage to the system, including cracks in any high-pressure fittings or fuel lines.
4. Open the water spigot on the wall and ensure water is flowing through the heat exchanger, checking for any major leaks.
5. Turn on the scale to ensure proper operation. This scale will later be used for fuel consumption data.
6. Switch on the lift pump and check the regulator to ensure a reading of approximately 24 psi.
7. Switch on the electric motor. No pressure rise should be shown on the large pressure gauge on the high pressure side of the plumbing. If a pressure rise does occur, immediately shut off the electric motor and check for proper functioning of the pressure relief valve on the rail. This valve should be open unless charged with 12 V.

8. Fuel should now be circulating through the common-rail and from the regulator. Now engage the pressure regulating valve on the common-rail. Pressure should rise to approximately 5000 psi. Adjust the pressure setting to the desired level using the controls on LabVIEW. **DO NOT ADJUST THE PRESSURE TO ABOVE 30,000 PSI.** Damage to the pump or injector could occur.
9. The fuel system is now prepped for operation. Crank the engine and run the desired experiments. If engine does not start, check to make certain the driving circuit for the injector is engaged properly. If the wire is disconnected, the injector will not deliver fuel and the engine will not run.

E.4.3 Budget for Common-Rail Injection System

Supplies that were not project specific

8841T4 terminal block, 5 circuit, 20 A	10	2.64	26.40
8841T7 DIN rail adapter for terminal block	20	0.92	18.40
8961K15 DIN 3 rail, 35 mm width, 1 m long	2	4.76	9.52
4704T212 HPLC lab bench, maple top	1	1,232.47	1,232.47
10365T71-regular-46 coveralls, long sleeve	1	38.38	38.38
10365T71-long-46 coveralls, long sleeve, tall version	1	38.38	38.38
53355T71-48 lab coat, long sleeve	1	27.60	27.60
5807A6 combo wrench set, 12 pc, 1/4" to 7/8"	1	42.41	42.41
5811A11 combo wrench set, 12 pc, 7 - 18 mm	1	42.40	42.40
85555A312 micrometer torque wrench, 3/8" drive	1	121.51	121.51
85555A318 micrometer torque wrench, 1/2" drive	1	144.62	144.62
9474T12 hydraulic pressure regulator, 500 - 2000 psi	1	191.21	191.21
76455A22 electrical tape	5	3.99	19.95
7007K92 wire stripper	3	13.26	39.78
6047A81 mallet, polyurethane head	1	28.76	28.76
3708K412 pressure gauge, 2000 psi, 4 1/2" dial	1	102.33	102.33
52245K824 SS tube fitting adapter for 3/8" tube to 3/8" MNPT	3	14.34	43.02

Shipping Subtotal	**150**
Subtotal NPSE	**2,317.14**

Supplies Specifically for This Project

6PG50 gage, 50000 psig, 1/2%	1	982.00	982.00
60-41HF4T soft-seat check valve	1	125.00	125.00
60-11HF4 high pressure valve	1	120.00	120.00
2-HF4L spare cutter	1	76.30	76.30
2-HF4P spare collet	1	57.20	57.20
1/4-28LH spare threading die	1	60.90	60.90
2-MHF4P spare guide bushing	1	27.50	27.50
60-2HM4 gland	4	5.50	22.00
60-2H4 collar	4	2.70	10.80
60-7HM4 plug	4	5.20	20.80
60-22HF4 elbow	4	34.20	136.80
60-23HF4 tee	2	48.80	97.60
60-63HF4 safety head tee type	1	130.00	130.00
60000-rupture-disk rupture disk, 60000 psi rating	2	41.30	82.60
60-HM4-12-304 nipple, 12", 304 SS	5	18.30	91.50
60-HM4-6-304 nipple, 6", 304 SS	5	12.50	62.50
60-9H4-304 1/4" OD high pressure tubing, 16 feet, cut into 8' lengths	16	9.30	148.80
60-21HF4-C cap	4	27.60	110.40
60-21HF4-U union	2	55.20	110.40
1863T82 10lb capacity digital scale	1	88.28	88.28
5839K12 20 amp extension cord, 25'	1	133.47	133.47
7087K35 fuse holder, 5x20 mm, panel mount	3	5.41	16.23

6978K77-10 fuses, 10A, 5x20 mm, pkg of 5	2	5.37	10.74
7798K42 3/4" electrical connector	4	1.15	4.60
7798K43 1" electrical connector	4	1.88	7.52
75065K35 steel enclosure, 6x6x6 with lift off cover	1	14.35	14.35
7798K44 1 1/4" electrical connector	4	3.93	15.72
7603K87 Enclosed motor controller 22-30 amp, non-reversing 120 VAC	1	377.28	377.28
6204K124 2 3/4" OD cast iron v-belt pulley 7/8" bore B-section	1	9.89	9.89
6204K391 7.75" OD cast iron v-belt pulley 5/8" bore B-section	1	35.60	35.60
6204K191 3.75" OD cast iron v-belt pulley 7/8" bore B-section	1	15.40	15.40
6209K224 8.95" OD cast iron bushing center v-belt pulley, B-section	1	43.08	43.08
162486 115 volt single-phase motor 1725 rpm capacitor start, 7/8" drive shaft	1	299.99	299.99
Common Rail Pressure Rail	1	450.40	450.40
High Pressure Fuel Injector	1	434.40	434.40
Common Rail High Pressure Pump	1	920.00	920.00
Fuel Line from Pressure Rail to Injector	1	48.40	48.40
Fuel Line from High Pressure Pump to Pressure Rail	1	74.10	74.10
Bleed Line from Rail	1	150.00	150.00

Shipping Subtotal	**400**
Subtotal PSE	**6,022.55**

USNA Costs (Machine Shop)	**Hours**	**Price/Hr**	
Machine Work on Head	2	$65.00	$ 130.00
Machine Work on Pulley	3	$65.00	$ 195.00
Machine Work on Base Plate	2	$65.00	$ 130.00
Machine Work on Brackets	3	$65.00	$ 195.00
Sheet Metal Work	1.5	$65.00	$ 97.50

Subtotal MSW	**$ 747.50**

USNA Costs (Materials)	**Units**	**Unit Price**	
Aluminum 3/8" plate	1	$140.35	$ 140.35
Aluminum 1/4" plate	1	$55.20	$ 55.20
Steel Sheet Metal 1/8"	1	$150.00	$ 150.00
Aluminum Structural Framing	1	$60.00	$ 60.00

Subtotal MSM	**$ 405.55**
Grand Total:	**$ 9,492.74**

Color Code	
High Pressure Equipment	
McMaster	
Northern Tool and Equipment	
Volkswagen	

Glossary

A

After Top Center (ATC): The crankshaft angular position after the piston reaches its highest point in the stroke.

B

Brake Mean Effective Pressure (BMEP): The work delivered to the crankshaft over the entire four strokes of the cycle, per unit displaced volume.

Brake Specific Fuel Consumption (BSFC): The fuel flow rate per unit power output as measured from the crankshaft.

Burn Duration: The length in crank angle degrees that it takes for the fuel to go from 10% combusted to 90% combusted.

C

Compression Ratio (CR): The ratio of the maximum cylinder volume to its minimum volume.

Clearance Volume (V_c): The minimum volume of the cylinder.

Crank Angle Degree (CAD): The angular position of the crankshaft with top dead center taken to be 000˚.

Crevice Volume: The volume inside the combustion chamber when the piston is at TDC.

D

Dynamometer: An instrument used for measuring power output, usually of an engine.

E

Enthalpy: The change in internal energy of a system plus the work that system has done on its surroundings.

F

Friction Mean Effective Pressure (FMEP): The work used to overcome friction in the engine over the entire four strokes of the cycle per unit displaced volume.

G

Gross Mean Effective Pressure (GMEP): The work delivered to the piston over the entire four strokes of the cycle, pre unit displaced volume. Also called indicated mean effective pressure (IMEP)

H

Heat Release (HR): The rate at which the fuel releases energy during the combustion process. HR is expressed in units of J/deg.

Heat Transfer Multiplier (HTM): In reference to the Ricardo Wave simulation, the contour line on which all engines have the same heat transfer characteristics. A HTM value of unity indicates the engine loses the same amount of heat as a standard automotive engine loses during similar operation.

I

Ignition Delay: The length in crank angle degrees that it takes for 5% of the fuel to combust measured from the start of injection.

Indicated Mean Effective Pressure (IMEP): The work delivered to the piston over the entire four strokes of the cycle, per unit displaced volume.

L

Low Heat Rejection (LHR): A property of an engine that has had materials with a low thermal conductivity applied to the combustion chamber in order to reduce the amount of heat released to the atmosphere.

M

Maximum Brake Torque (MBT): The maximum amount of torque that can be produced on the crankshaft for a given amount of fuel.

N

Net Mean Effective Pressure (NMEP): The net work delivered to the piston over the entire four strokes of the cycle, per unit displaced volume, found by subtracting the work to overcome friction (FMEP) from the indicated work (IMEP).

P

Peak Pressure Location (PPLOC): The crankshaft angular position at which the peak pressure occurs during the combustion event.

S

Sauter Mean Diameter: An average particle size, referring to the droplet's diameter.

Squish (Height): The area between the flat of the piston and the flat of the cylinder head at top dead center (TDC)

Start of Injection (SOI): The crank shaft angular position at which fuel begins to spray into the cylinder. Top dead center is taken to be an angular position of 000˚.

T

Thermal Barrier Coatings (TBC): A material with a low thermal conductivity that can be applied in a thin coating on the combustion chamber of an engine in order to reduce the amount of heat lost to the atmosphere.

Thermal Impedance: A material property that relates the ease at which heat is transferred conductively through the material. High thermal impedance indicates a low rate of heat transfer.

Top Dead Center (TDC): The crankshaft angular position when the piston is at its highest point of travel. This position is the general reference to all other numerical values for crankshaft angular position.

W

Woschni Correlation: An expression used to determine the heat transfer coefficient while taking into account changes in gas velocity throughout the cycle.